Selective and Sensitive Determination of Real-Time Butyrylcholinesterase Activity via Phenoxy 1,2-dioxetane-based Chemiluminescent Probe

by

ALPEREN ACARI

A Dissertation Submitted to the
Graduate School of Health Sciences
in Partial Fulfillment of the Requirements for
the Degree of

Master of Science

in

Cellular and Molecular Medicine

April, 2023

Selective and Sensitive Determination of Real-Time Butyrylcholinesterase Activity via Phenoxy 1,2-dioxetane-based Chemiluminescent Probe

Koç University

Graduate School of Health Sciences

This is to certify that I have examined this copy of a master's thesis by

ALPEREN ACARI

and have found that it is complete and satisfactory in all respects,
and that any and all revisions required by the final
examining committee have been made.

Committee Members:

_____

Assist. Prof. Dr. SAFACAN KÖLEMEN (Advisor)

_____

Prof. Dr. TUĞBA BAĞCI ÖNDER

_____

Assist. Prof. Dr. SÜNDÜS ERBAŞ ÇAKMAK

Date: _____

Dedicated to the Martyrs of Dardanelles

“Sana dar gelmeyecek makberi kimler kazsın?

′Gömelim gel seni tarihe′ desem, sığmazsın.”

“Who can dig the grave which will not be narrow for you?

If I said “lets burry you into history”, you wouldnt fit into”.

ABSTRACT

Selective and Sensitive Determination of Real-Time Butyrylcholinesterase Activity via Phenoxy 1,2-dioxetane-based Chemiluminescent Probe

ALPEREN ACARI

Master of Science in Cellular and Molecular Medicine

April, 2023

Butyrylcholinesterase (BChE), or pseudo-cholinesterase, is one of the significant cholinesterases in the human body with a diverse substrate range and function area. It plays crucial roles in numerous physiological and pathological processes, including regulation of acetylcholine, detoxification of poisons, metabolism of drugs, regulation of fat metabolism, and beyond. Accordingly, it is an essential yet challenging target for bioimaging studies. Several methods and small molecule probes have been proposed for BChE activity detection and measurement so far. However, they suffered from either low detection limits, inadequate selectivity or method-intrinsic drawbacks. Herein, we have presented a BChE-responsive chemiluminescent probe, BCC, based on a phenoxy 1,2-dioxetane core with an electron-withdrawing acrylic group for monitoring BChE activity in native biological contexts; thus, we have introduced the first-ever example of a chemiluminescence-based bioimaging technic for the visualization of BChE activity. BCC generated a selective and sensitive turn-on response with BChE but not with competitive analytes in aqueous solutions. BCC was successfully utilized to measure and visualize endogenous BChE activity in normal and cancerous cell lines without showing any toxicity. Inhibition studies have proven that BCC can detect fluctuations in BChE levels precisely. BChE in healthy mice models has been visualized in distinct body regions, from the liver to the brain, as BCC could pass through the blood-brain barrier. Likewise, tumours grown on mouse models derived from neuroblastoma cells have been pictured with a very high signal-to-noise ratio. Hence, BCC stood out as a promising chemiluminescent probe for selective and sensitive detection of BChE, which can be used to further understand its contribution to regular biological processes and the formation of diseases.

ÖZETÇE

Fenoksi 1,2-dioksetan Temelli Kemilüminesan Ajan Kullanımıyla Gerçek Zamanlı Butirilkolinesteraz Aktivitesinin Seçici ve Hassas Tayini

ALPEREN ACARI

Hücresel ve Moleküler Tıp, Yüksek Lisans

Nisan, 2023

Butirilkolinesteraz (BChE), ya da diğer adıyla psödo-kolinesteraz, geniş substrat aralığı ve kapsayıcı fonksiyon alanı ile insan vücudundaki önemli kolinesterazlardan biridir. Asetilkolinin düzenlenmesi, kimyasalların ve ilaçların detoksifikasyonu ile yağ metabolizmasının düzenlenmesi dahil olmak üzere çok sayıda fizyolojik ve patolojik süreçte kritik roller oynar. Bu sebeple, biyogörüntüleme çalışmaları için kıymetli, ancak zorlu bir hedeftir. Bugüne kadar BChE aktivitesinin tespiti ve miktarının doğru ölçümü için çeşitli yöntemler ve küçük molekül yapılı ajanlar önerilmiş olmakla birlikte, bunlar düşük ölçüm limitlerinden, yetersiz seçicilikten ya da yöntemlerin kendine özgü dezavantajlardan muzdariplerdir. Biz bu çalışma ile elektron çekici bir akrilik grubu taşıyan fenoksi 1,2-dioksetan yapıya sahip ve BChE'ye oldukça duyarlı bir kemilüminesan ajanı, BCC'yi, sunuyoruz. Bu ajan, BChE aktivitesinin görselleştirilmesi için geliştirilmiş kemilüminesan tabanlı biyogörüntüleme tekniklerinin ilk örneğini olma onuruna sahiptir. Sulu ortamdaki çalışmalarımız boyunca, BCC BChE'ye karşı oldukça seçici ve hassas bir reaksiyon sergiledi, ama rekabetçi analitlerle tepkimeye girmedi. BCC, herhangi bir toksisite göstermeden normal ve kanserli hücre hatlarında endojen BChE aktivitesini ölçmek ve görselleştirmek için başarıyla kullanıldı. İnhibisyon çalışmaları BCC'nin BChE seviyelerindeki dalgalanmaları kesin olarak tespit edebildiğini kanıtladı. BChE, sağlıklı fare modellerinde karaciğerden beyne kadar farklı vücut bölgelerinin görselleştirilmesini sağladı ve kan-beyin bariyerinden geçebildi. Benzer şekilde, fare modellerinde nöroblastoma hücreleri kullanılarak üretilen tümörleri çok yüksek bir sinyal/gürültü oranıyla görüntüleyebildi. Bu sonuçlar göz önüne alındığında, BCC BChE'nin biyolojik süreçlere ve hastalıkların oluşumuna olan katkısını daha iyi anlamak için kullanılabilecek, seçici ve hassas bir kemilüminesan ajan olarak öne çıkmaktadır. Umudumuz BCC'nin klinik ve araştırmalarda ileri uygulamalara katkıda bulunabilmesidir.

ACKNOWLEDGEMENTS

You need luck more than good ideas and hard work for academic success. My luck in this journey was in the people I worked with, who held my hand every time I got exhausted.

First, I thank my advisor Dr Safacan Kolemen for being more than a P.I. throughout the years we spent in my graduate and undergraduate life. He was with me in every milestone, added value to my life and helped me to solve many academic and personal problems in his unique style. I desire a long-standing relationship with him that has gone even deeper after my graduation.

Next, I would like to thank Musa Dirak for being one of a kind lab partner. I would go with you all the way, yet there is no reality where I have as much energy as you. I know you will succeed so much but get rest sometimes. We have a long friendship to continue. Likewise, Toghrul Almammadov, an old friend, deserves so many compliments with his pure heart. He taught me the basics along with Safacan Hoca and guided me throughout this journey. I also thank Toghrul for the synthesis of compound 1. I was not the only one who got his share from Toghrul. Berkan Bozkurt accompanied me all the way from start to end. Your companionship was precious, thank you. I also want to thank Ayca Saymaz for being there whenever I need, and my beloved Kolemenlab partners Dr Hande Gunduz, Dr Aatif Ijaz, Dr Hamdiye Yadigar Ece, Kubra Durgun, Muserref Cansu Yenici, Ceren Unver, Mehmet Akif Aktas, Sarp Emre Turan and Mina Mustafazade for their precious help.

Another person I appreciate so much is Beyza Nur Koseoglu. She gave too much of her time to help me progress academically and personally. I wish to repay somehow, but only sky is the limit for Beyza's good intentions and self-sacrifice. Dr Ahmet Cingoz and Nareg Degirmenci were with me throughout this journey, starting from the very beginning. Their experience and expertise contributed much to my development, and their work always set an example for me. Dr Cingoz taught me everything I know in terms of animal handling and performing *in vivo* experiments. I also want to thank my beloved friends Beril Esin, Ebru Yilmaz, Dr Ozlem Yedier Bayram, Goktug Karabiyik, Ezgi Yagmur Kala, Canan Bayraktar, Fulya Mina Kucuktas and Gizem Dogan Yilmaz in the

TBO lab. I need a special thanks to Dr Tugba Bagci-Onder itself. She always shared her precious time and guided me with her valuable thoughts.

Furthermore, Dr Oykum Kaplan-Arabaci always became a great mentor of mine and encouraged me to do what was in my heart. Her valuable ideas took me out of the darkness and helped me walk confidently towards my ideal. Pinar Ciftci was a priceless lab partner ready to work hard no matter what and supported me in every condition with her strong will and hope. I want to thank Dr Nesibe Peker and Dr Yunus Akkoc, who mentored me in this journey with invaluable thoughts and help. I also want to thank priceless friends of mine, Ayse Seray Guzel, Eren Yukseloglu, Gamze Deveci, Irem Yenidogan, Ramiz Demir, Sahra Aras and Sıla Turgut in the Gozuacik lab. I thank Dr Devrim Gozuacik for teaching me an important life lesson. There is always light behind dark days.

My beloved family, mother, father and sister gave all the support they could. I couldn't have come this far without their support. I want to add another special thanks to my uncle Serkan Karadayı for being there whenever I need and picking me up every time I broke apart. And, I thank the rest of my family for supporting me in every step and sharing this journey.

Finally, I thank Bensu. She needs no fancy words.

TABLE OF CONTENTS

LIST OF TABLES

LIST OF FIGURES

ABBREVIATIONS

a.u.	Arbitrary Unit
ACh	Acetylcholine
AChE	Acetylcholinesterase
AD	Alzheimer's Disease
ATP	Adenosine Triphosphate
AUC	Area Under the Curve
BBB	Blood-Brain Barrier
BCC	Butrylycholinesterase Selective Chemiuminscent Probe
BChE	Butyrylcholinesterase
ChE	Cholinesterase
CIEEL	Chemically Induced Electron Exchange Luminescence
CTG	Cell Titer-Glo® Luminescent Cell Viability Assay
DMEM	Dulbecco's Modified Eagle Medium
DMSO	Dimetyl Sulfoxide
DPBS	Dulbecco's Phosphate Buffered Saline
DTNB	5,5'-Dithiobis-2-Nitrobenzoic Acid
ELISA	Enzyme-Linked Immunosorbent Assay
FBS	Fatal Bovine Serum
GHS-R	Growth Hormone Secretagogue Receptor
HR-MS	High Resolution Mass Spectrometry
IC_{50}	Inhibition Coefficient
IP	Intraperitoneally
LBD	Lewy Body Dementia
NIR	Near-Infrared Light
NMR	Nuclear Manyetic Resonance
NOD/SCID	Non-Obese Diabetic/Severe Combined Immunodeficiency
PD	Parkinson's Disease
PDD	Parkinson's Disease Dementia
RLU	Relative Light Units
ROI	Region Of Interest
SPN	Semiconducting Polymer Nanoparticles
Tacrine	9-Amino-1,2,3,4-Tetrahydroacridine Hydrochloride Hydrate
TLC	Thin Layer Chromatography
TNB	5-Thio-2-Nitrobenzoic Acid

Chapter 1:
INTRODUCTION

1.1 Butyrylcholinesterase

Cholinesterases (ChEs), hydrolyzing choline esters to alcohol and acid (Figure 1.1), are a crucial group of carboxylesterases with a significant function in neurotransmission, and acetylcholine, created and discharged by neurons to transmit nerve signals, is their primary target in the body. There exist two members of the family that are acetylcholinesterase (AChE), honored as "true" and "specific" cholinesterase because of high specificity against acetylcholine, and butyrylcholinesterase (BChE), recognizing broader substrate group and known as "pseudo" or "non-specific" cholinesterase[1–6]. Although AChE and BChE have similar structures and catalytic functions, they have distinctive tissue distribution, substrate specificity, inhibitor sensitivity, and physiological purposes[7]. AChE is a high-turnover enzyme located in the central and peripheral nervous system and inhibited by high acetylcholine concentrations as an example of substrate inhibition, despite being famous for showing a spectacular affinity and specificity for acetylcholine[4,8,9]. In contrast, BChE is present in most tissues with a greater concentration in the serum and liver[1–4,7]. It has a weaker affinity for acetylcholine with a slower reaction rate and can break down both choline and non-choline (aliphatic) esters[4,8]. Still, BChE is a significant component of the central and peripheral nervous systems and plays a vital role in acetylcholine regulation[1–4,7].

It is only accurate to say that the role of BChE is not limited to the inactivation of acetylcholine but includes detoxification of poisons, metabolism of drugs, regulation of fat metabolism, and beyond[1,4,5,10–14]. However, the understanding of BChE's importance beyond supporting AChE wasn't until the broad application of succinylcholine as an anesthesia agent. It quickly realized that the longer recovery time of some patients after succinylcholine administration was due to their low serum BChE activity[15–17]. That realization led to further investigation of BChE with various organophosphorus compounds, such as nerve agents (sarin, tabun) and pesticides (paraoxon, malathion), which revealed that the so-called pseudocholinesterase had a much broader range of

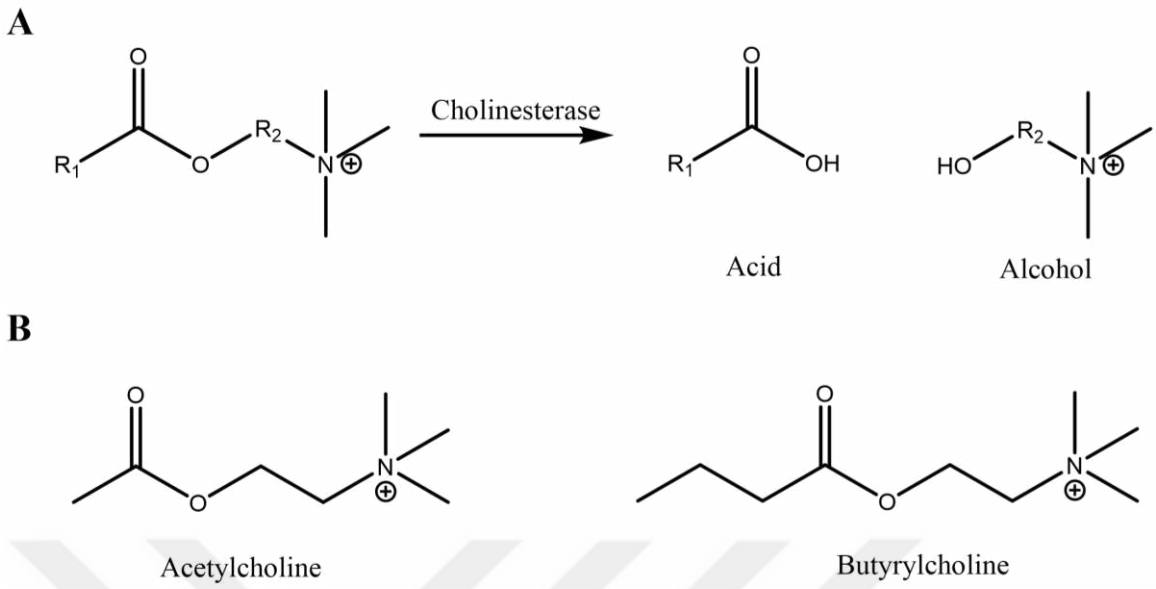

Figure 1.1: A) Reaction of Cholinesterase, B) Acetylcholine and Butyrylcholine.

substrates than just choline esters[18,19]. Following that, numerous studies have linked BChE to Alzheimer's disease, which is present in the amyloid-beta plaques developed in the brain[20,21]. Research on Parkinson's disease showed patients with dementia have higher BChE levels than those without dementia[22,23]. Cancer studies have shown a strong correlation between abnormal BChE expression and tumorigenesis[24–26], where elevated tumor-associated BChE expression induced neuroblastoma development[27]. Furthermore, increased BChE activity is connected directly to insulin resistance and diabetes, obesity, liver damage, cardiovascular disorders, and uremia[28–30].

1.1.1 BChE and Neurodegenerative Diseases

Neurodegenerative diseases originate from the gradual disintegration of the neuronal structures, and low acetylcholine levels accompany that as an indicator of disrupted cholinergic pathways vital for optimal brain function. The resulting cognitive impairments cause severe pathological outcomes that lower the life quality of patients. Although the main effort is on regulating AChE activity to treat the consequences of the diseases, BChE has an unignorable effect on neurodegenerative disease development due to its role in acetylcholine regulation, especially in Alzheimer's and Parkinson's Diseases.

Alzheimer's Disease

AChE is the primary enzyme involved in cholinergic neurotransmission under normal circumstances, but acetylcholine levels are not sufficient under disease conditions to regulate normal brain functions. A promising treatment option was to use AChE inhibitors to decrease acetylcholine hydrolysis and ensure a stable level of acetylcholine[21,31]. However, the use of AChE-specific inhibitors had a limited effect on Alzheimer's Disease (AD) patients and was inadequate to relieve cognitive and behavioral symptoms[31,32]. As BChE activity can balance the decreased function of AChE in hydrolyzing acetylcholine, recent research attempted to inhibit BChE as a compensatory method, resulting in a 5-fold increase in acetylcholine levels at the study of Hartmann et al. in AChE-knockout mice[33]. A separate work found that BChE-knockout mice with Alzheimer's disease had reduced amyloid-beta plaque deposition, suggesting that BChE activity may stimulate the maturation of this plaques[34]. Further, brain samples obtained from an old age group of patients with and without Alzheimer's disease have shown abnormal aggregation of BChE in mature amyloid-beta plaques[20]. Additional research is needed to reveal the exact role of BChE in Alzheimer's disease; however, the compensatory activity of BChE and its accumulation in plaques make this pseudocholinesterase an attractive diagnosis and prognosis tool in the eyes of many researchers.

Parkinson's Disease Dementia and Lewy Body Dementia

Parkinson's disease (PD) involves the death of dopaminergic neurons and the formation of alpha-synuclein aggregates (Lewy bodies)[23,35]. Patients with PD are 2 to 6 times more likely to develop dementia, resulting in Parkinson's Disease Dementia (PDD)[35]. Lewy body dementia (LBD) is another type of dementia where alpha-synuclein aggregates accumulate in the brain[36]. Both PDD and LBD involve a loss of cholinergic activity in the brain, but they differ from Alzheimer's disease in terms of the specific protein that causes the pathology. Caballol et al. found that LBD patients have lower BChE activity in serum compared to Alzheimer's disease patients and healthy individuals[35]. PDD patients show similar low BChE levels compared to Parkinson's disease patients without dementia[23]. Due to its association with the progression of PDD

and LBD, the detection of BChE activity has emerged as a potential biomarker for both conditions.

1.1.2 BChE and Ghrelin

Ghrelin is a multi-purpose hormone regulating hunger, energy metabolism, insulin and glucose homeostasis, and award perception[3,5,30]. BChE is known to participate in ghrelin regulation by hydrolyzing the octanoyl group needed for ghrelin activity at the growth hormone secretagogue receptor (GHS-R)[37,38]. Dorling et al. revealed that low levels of BChE in plasma drove a higher ghrelin/desacyl-ghrelin ratio and hypothesized that BChE serves a role in energy metabolism regulation through ghrelin, increasing adiposity and long-term weight gain at inadequate levels[39]. Further studies by Chen et al. showed that BChE knockout mice tend obesity more than the control group[40]. On top of it, the peripheral expression of BChE reduced the effect driven by the lack of BChE almost entirely, supporting the role of BChE in the regulation of fat metabolism and accumulation[40,41]. It has been showed that ghrelin has a negative effect on insulin secretion in rats and mice[41] and impairs glucose tolerance in humans[40]. These findings may point out the role of BChE in insulin and glucose homeostasis through a BChE-ghrelin pathway, yet further research is required to understand the involved mechanisms. Other than this, studies by Spencer et al. proved the influence of ghrelin on mood-related behaviors in mice, such as anxiety[42]. Moreover, mice lacking the BChE gene showed significantly more aggressive behavior than normal mice in the studies of Chen et al., while increasing the amount of BChE in their blood reduced the aggression[41].

To summarize, BChE plays a role in regulating fat metabolism and behavior through the ghrelin signaling pathway. Other medical conditions, such as post-traumatic stress disorder, were also attributed to abnormal BChE activity on ghrelin. Although it still requires further understanding, it is apparent that BChE might be a promising tool in diagnosing a wide range of disorders, varying from obesity to psychological disorders.

1.1.3 BChE and Detoxification

The high levels of BChE in the human body and its presence in the liver, lungs, and serum indicate that it may function as a detoxifying enzyme [43,44]. In line with this, studies

revealed that BChE activity levels are lower in people exposed to organophosphate pesticides[45]. Moreover, BChE-administered animals were protected from toxicity when exposed to nerve agents[46], while BChE-knockout mice had an additional vulnerability to poisoning by the same agents[47]. AChE-knockout mice showed similar vulnerability, probably because BChE was occupied with stabilizing the ACh level, thereby disrupting its detoxifying function[48]. BChE is known to react with a broad range of substrates due to the considerably large acyl pocket size in the enzyme active site. It has a comprehensive substrate range, including conventional anti-ChE agents such as organophosphate pesticides and, surprisingly, drugs like cocaine and heroin, as BChE converts cocaine to ecgonine methyl ester, removing its toxicity[49,50]. In a study, BChE-administrated animals managed fatal outcomes of lethal doses of cocaine without seizures, while the untreated group harmed[51]. Further analysis exhibited that the cocaine levels were four times lower in the BChE-treated group in the brain and plasma compared to untreated ones[51]. Therefore, the BChE administration is a promising tool for dealing with cocaine overdose-caused deaths and cocaine addiction.

Besides artificial ones like pesticides, several natural anti-ChEs are present in the environment, including alkaloids, carbamates, and hormones, which are plant metabolites serving as chemical defenses against herbivores. The consumption of these natural anti-ChEs in the diet is known to impact BChE activity, where eating potatoes decrease serum BChE activity in humans and influence the effect of drugs[52]. This effect of plant-based anti-ChEs served as a foundation for developing medicines used to treat Alzheimer's disease, as they reduce the activity of BChE and increase the available concentration of ACh indirectly[53–55]. Yet, long-term exposure to anti-ChEs has been associated with several unhealthy consequences, including cancer development and direct DNA damage[56–58]. Anti-ChE exposure during pregnancy may cause embryonic malfunction and possible birth defects[59–61]. Considering this, it is crucial to detect the presence of anti-ChEs, and there is a need for sensitive and selective tools.

BChE meets the characteristics of a detoxification enzyme according to Ziegler's fourth criterion, including the ability to bind to a wide range of substrates, high concentrations in the entry organs, inducibility, and variation in concentration across species based on their particular diets[62]. BChE reacts with pesticides, alkaloids,

carbamates, plant hormones, and more[5,6,45,63,64]. Although BChE plays essential roles in the central nervous system, it is concentrated in the lungs, blood, and liver and has critical functionality [43,44]. The serum expression is inducible by exposure to anti-ChE agents, and its concentration differs across species[46,65]. Therefore, BChE is indeed a detoxification enzyme; thus, sensitive, and selective measurement of its activity may be a promising tool for toxin identification.

1.1.4 BChE and Cancer

There is no doubt that further research is required to fully understand the relationship between BChE activity and cancer formation, as it is a multifaceted topic. However, several studies have already suggested that abnormal levels and activity of BChE are associated with cancer. For instance, research showed that low serum BChE activity implies a dysfunctional liver and a marker of possible liver cancer[66]. Some other studies similarly reported low serum BChE in cancer patients, but the underlying mechanisms still need clarification[25,67]. Beyond that, high local BChE activity has been suggested as a prognostic marker for cervical and oral cancers as BChE activity increases during tumor development in later stages[26,68]. Gu et al. reported downregulation of BChE expression in the early stages of prostate cancer and upregulation at further stages[69]. According to Onder et al., BChE is not secreted in neuroblastoma cells but is found active within the cytoplasm[27]. Another group reported a positive correlation between tumor growth and increased BChE levels in type IV glioma[24]. From a superficial perspective, BChE activity is supposed to reduce the likelihood of cancer formation due to its detoxification effect; however, the relationship between BChE activity and cancer formation looks like a more complex issue that requires further investigation.

In summary, BChE is a significant cholinesterase with a wide range of substrate pool and body distribution, vital regulatory and detoxification roles, and an unfortunate contribution to disease formation under abnormal activity. It is not an unfunctional sister of acetylcholinesterase, but a strong partner of it. Understanding the roles of BChE in different organs and the pathways it follows throughout our metabolism is of great importance to solving the unknowns of many diseases.

1.2 Chemiluminescence

Chemiluminescence is the emission of light based on a chemical reaction producing an electronically excited molecular state, which emits light while relaxing to the ground state. Many forms of chemiluminescent light exist in nature and chemistry. On the one hand, luciferin-luciferase-based biological chemiluminescence, also known as bioluminescence, is observed in species such as fireflies, jellyfish, and single-cell marine organisms[70–72]. On the other hand, there are ozone-based, luminol-based, imidazopyrazinone-based, peroxyoxalate-based, and 1,2-dioxetane-based sources of non-biological chemiluminescence[73–81]. Countless applications of both bioluminescence and non-biological chemiluminescence have been adapted to molecular biology and analytical chemistry fields. The earliest adaptations in molecular biology include but not limited to western blotting, immunoassays, viability assays, and DNA sequencing, which are all essential tools today. Yet, chemiluminescence always had a broader application potential that stayed hidden due to some limitations of the early agents and could only be revealed today. Currently, it has been utilized to detect and quantify several organic and inorganic analytes, where some are biomarkers of diseases, pathological abnormalities, and cancer onset[74,80]. Chemiluminescent imaging techniques are considered superior to many other prior methods, including fluorophore-based ones. Compared to fluorescence, where the signal is emitted upon irradiation, chemiluminescence does not require an external light source. Henceforth, it solves several chronic drawbacks of the conventional fluorophores, such as limited penetration of the excitation light, photobleaching, autofluorescence, and low signal-to-noise ratios, especially *in vivo* studies.

1.2.1 1,2-dioxetane-based Chemiluminescence

Although chemiluminescent probes are now valuable tools for the real-time visualization of enzyme activities and detection of biologically significant analytes, their applicability in biological systems is recent. Among all proposed chemiluminescent scaffolds, the 1,2-dioxetane-derived core offered for the first time by Schaap et al. in 1987[82–84] (Figure 1.2) stood out with the best biological applicability especially after the improvements done by Shabat et al. in 2017[81].

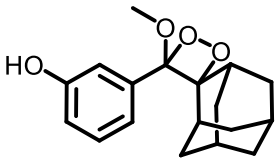

Figure 1.2: Schaap's scaffold for chemiluminescence.

The activation mechanism of Schaap's dioxetane is initiated upon deprotection of the caging group attached to the phenolic hydroxyl, which subsequently triggers the chemically induced electron exchange luminescence (CIEEL) mechanism and releases a chemically excited benzoate that emits light during relaxation (Figure 1.3)[72,85,86]. The exact mechanism of the chemiluminescent light formation in phenoxy 1,2-dioxetanes was not fully understood yet, but CIEEL is the most appreciated pathway in the literature for chemiluminescent light generation (Figure 1.4). Upon deprotection, intramolecular electron transfer occurs from hydroxyl anion to cyclic peroxide bond, resulting in biradical intermediates that are converted to excited benzoates after back-electron transfer and emitting light as a result of the relaxation process.

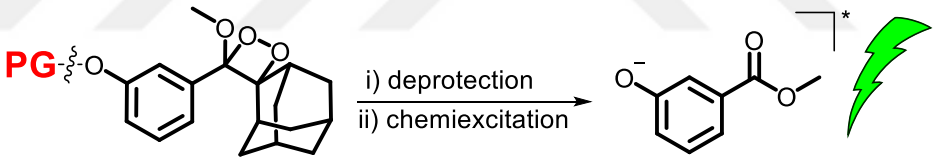

Figure 1.3: Activation mechanism of chemiluminescence.

Although Schaap's design looked promising as it increased the yield of emissive singlet excited state molecules upon deprotection and chemiexcitation steps, it was unsuccessful in aqueous media contrary to expectations due to the high pKa of its hydroxyl group. An improved chemiluminescence quantum yield was needed to utilize this scaffold *in vitro* and *in vivo* applications; hence, Schaap's scaffold lacked biological applicability at the time. However, Schaap's impact on developing a universal chemiluminescent core by using phenolate-attached dioxetanes was tremendous and introduced a method to increase emissive singlet excited state molecules and lower non-emissive triplet excited state.

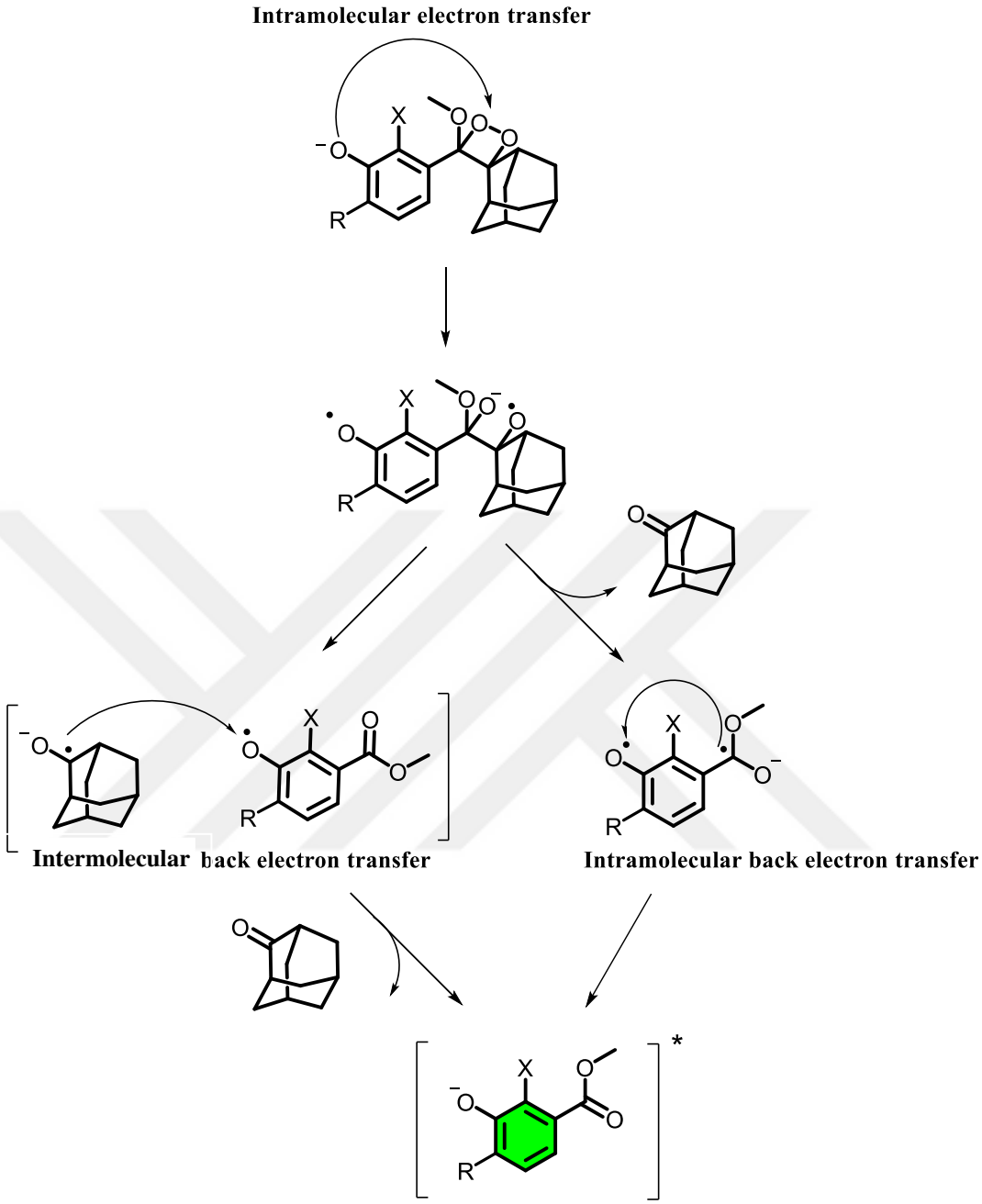

Figure 1.4: Proposed mechanism for CIEEL (X=Cl, R=EWG).

One proposed solution to introduce a chemiluminescent scaffold that works in physiological pH was ortho-chlorinating the hydroxyl group of Schaap's design to decrease the pKa[87]. However, the chemiluminescence intensity remained scarce in aqueous solutions even after modifying the ortho position. Fortunately, the chemiluminescence quantum yield was dramatically increased once the other ortho position was conjugated with an electron-withdrawing acrylate groups, according to the

study of Shabat's group in 2017[81]. A 3000-fold enhancement was detected in the chemiluminescence signal intensity, making it sufficiently detectable in aqueous environments, thus, in biological systems (Figure 1.5). This modification created a strong push-pull system as in the case of bright conventional fluorophores and further decreased the pKa of the phenol and consequently increased the phenolate concentration at pH 7.4.

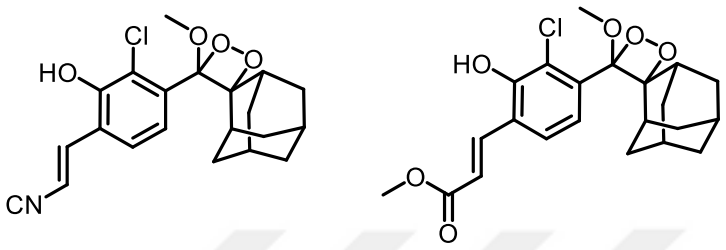

Figure 1.5: Electron withdrawing group conjugated chemiluminescence scaffolds.

Once an innovative chemiluminescence scaffold that produces strong signal intensities in aqueous environments was developed, several adaptations were designed to visualize biologically significant analytes in real time. In 2017, the Shabat group combined chemiluminescence core with cell-penetrating peptide to assess $^1O_2$ activity in HeLa cells. In the presence of $^1O_2$, 1,2-dioxetane was formed *in situ* and subsequently decomposed into excited benzoate following the CIEEL mechanism[88]. After a short time, the Shabat group introduced the first non-luciferin chemiluminescent activatable small molecule probes to detect hydrogen peroxide, glutathione, β-Galactosidase, and alkaline phosphatase[81]. Following that, a chemiluminescent agent selective for Cathepsin B, an enzyme known to be overexpressed in breast, colon, lung, and ovarian cancer, was developed, portraying the potential of small molecule chemiluminescent probes to detect diseases[26]. Afterward, several highly selective and sensitive imaging agents were designed to detect important enzymes, including tyrosinase, carboxyl esterase, nitroreductase, leucine amino peptidase, and more[89–95]. There were also studies to develop 1,2-dioxetane-based probes to detect biologically significant analytes, including reactive oxygen species such as H_2O_2, HOCl, HNO, O_2, $O_2^{\bullet-}$ and $ONOO^-$ [81,96–103] as well as biothiols such as H_2S, Cys, and GSH[87,104–106]. Even change in the pH became detectable by chemiluminescent probes[107].

The core of Schaap's produces a chemiluminescence signal at the 520 nm region of the light spectrum, where biological substrates may absorb the resulting emission. Recent applications proved that once the chemiluminescence core is conjugated with a red-emitting dye, its emission shifts to the near-infrared region, enhancing the chemiluminescent signal's penetration depth and increasing its applicability *in vivo* usage as in the study of Hananya et al., where their group developed a NIR-shifted β-Galactosidase selective chemiluminescent probe through the attachment of quinone-cyanine fluorophore[108]. In another study, Green et al. directly modified the dioxetane scaffold to form an extended π-electron system and proposed two new NIR chemiluminescent probes for detecting β-Galactosidase and hydrogen peroxide[109]. For the sake of red shifting the chemiluminescent signal, researchers also adapted semiconducting polymer nanoparticles (SPN), where Cui et al. developed the near-infrared chemiluminescent probe SPNR3 for detection of $O_2^{\bullet -}$ that emits light at 700 nm[110]. Supramolecular complexes were another promising alternative, as seen in the study of Gnaim et al., where they formed a fluorogenic dye-tethered cyclodextrin complex with the dioxetane core[111]. Additionally, some other studies showed that the chemiluminescence ring could be replaced with a cyanine scaffold to retrieve a shift in emission toward the NIR region[112].

In summary, a novel strategy has been proposed after combined efforts of Schaap and Shabat to develop non-biological chemiluminescent probes with high emission efficiency under physiological conditions. The approach aims protection of the phenol attached to an adamantylidene–1,2-dioxetane. The protected core structure stays inactive until the cleavage of the masking unit and only produces a chemiluminescent signal after the deprotection and decomposition of the 1,2-dioxetane. New generation 1,2-dioxetane based chemiluminescent probes have proposed high stability, selectivity, sensitivity, and bright signal intensities under physiological conditions. These agents have shown great potential as diagnostic and theranostic tools for several pathological diseases as they overcome the limitations of their alternatives, especially fluorophores, by eliminating the external excitation requirement. Yet, there is still a need to develop 1,2-dioxetane-based chemiluminescent probes for other biologically significant components, including BChE itself.

1.3 Developments in the BChE Quantification and Visualization

Various methods have been used to measure butyrylcholinesterase activity, including spectrophotometric, fluorometric, and electrochemical assays. The most commonly used method is Ellman's colorimetric assay, which involves hydrolysis of a thiocholine-derivative by cholinesterases and the reaction of hydrolysis product with thiol reagent 5,5'-dithiobis-2-nitrobenzoic acid (DTNB), leading to the formation of 5-thio-2-nitrobenzoic acid (TNB) anion[113]. Acetyl or butyryl derivatives of thiocholine are used according to the type of cholinesterases that will be measured, either AChE or BChE. The TNB ion's absorption is measured for BChE at 410 and AChE at 440 nm to determine the ChE activity indirectly. However, investigations have pointed out that Ellman's method may not be accurate enough for measuring ChE activities since it is an indirect method, and the assay generates a signal for both AChE and BChE with low sensitivity[114–117].

Besides Ellman's method, some other ways to detect BChE exist, including paper-based models, electrochemical techniques, and enzyme-linked immunosorbent assay (ELISA)[118,119]. Some researchers developed BChE activity assays based on enzyme activity-sourced acetic acid release and consequent pH change[120–122]. The pH indicator filter papers changed color gradually based on the concentration of the released acetylcholine. Yet, these assays were far from being sensitive. Some additional studies focused on inhibitor usage and tried to use different combinations of AChE, BChE, and double-selective inhibitors to increase detection sensitivity[123]. Scheller's group designed a piezoelectric biosensor based on real-time measurement of the BChE-inhibitor interaction using a paraoxon-modified surface [124]. There were investigations on developing a radiometric assay by Johnson et al.[125]. Pohanka has proposed a voltametric-based method using cholinesterasemia to overcome the instability of 5,5'-dithiobis-2-nitrobenzoic acid used in the Ellman's method[126]. Although its approach has provided a practical detection limit, AChE- and organic solvent interference has been detected. Polyclonal rabbit antibodies were developed by Norgaard-Pederson and Saphier groups for ELISA-dependent human BChE quantification[127,128]. These approaches were advantageous in terms of easy-to-use structure, yet they were costly methods and offered low selectivity and sensitivity compared to fluorophores mentioned below.

Fluorescence imaging is quite appealing to monitor BChE activity as it enables real-time imaging in a native biological medium with a high spatial and temporal resolution. To this end, various small activity-based fluorescent probes have been developed for both *in vitro* and *in vivo* imaging of BChE activity[129–138]. In 2017, Yang and colleagues introduced an exceptional study, a fluorescein derivative carrying a cyclopropyl masking unit was developed as a highly selective BChE probe, which displayed an insignificant signal in the presence of AChE, a genuine competitor[129]. Then, NIR fluorescent probes were synthesized using the same cyclopropyl unit to image BChE activity in Alzheimer's disease-bearing mice brains[130,139]. Recently, Liu and Qin proposed a similar probe structure to monitor BChE in different cells and mouse models[140]. Several other probe designs were successfully utilized to detect BChE activity in zebrafish models with high selectivity and sensitivity[133,134,141]. Although not all the probes have contained the cyclopropyl moiety developed by Yang, the ones bearing it attracted great attention in terms of selectivity. Yet, even though the fluorescent probes have been utilized successfully to image real-time BChE activity in biological environments, they still intrinsically maintain the chronic drawbacks of fluorescence, such as limited penetration of the excitation light, photobleaching, autofluorescence, and low signal-to-noise ratios, especially *in vivo* studies. To address the problems that conventional fluorophores are facing, phenoxy 1,2-dioxetane-based chemiluminescent probes appear as a promising alternative. These new generation probes offer very high sensitivity and signal to noise ratios under physiological conditions. Furthermore, they can be easily converted to triggerable activity-based probes by simply masking the phenol group with a cage unit that can be removed selectively.

Considering the contribution of BChE to physiological and pathological processes, it is of great importance to monitor BChE activity, changes in its concentration, and spatial/temporal distributions in living cells and the body with high selectivity and sensitivity to increase our understanding of BChE and, hopefully, develop potential applications to use in research and clinic. This study aimed to create the first-ever example of a BChE-responsive 1,2-dioxetane derivative for *in vitro* and *in vivo* visualization of BChE activity. Our probe BCC is a new-generation chemiluminescent probe carrying an electron-withdrawing acrylonitrile group, which is necessary to get bright a luminescence under physiological conditions. The presence of the acrylate group forms a push-pull type

luminophore and enhances the phenolate concentration in aqueous solutions at pH 7.4 by decreasing the pK_a of the phenol. BCC also carries a cyclopropyl moiety on the phenol part as a BChE-responsive caging group to get selectivity towards BChE. BCC was not luminescent in its caged form, yet, the cage group was cleaved selectively upon reacting with BChE, followed by the chemiexcitation generating a bright luminescent signal.

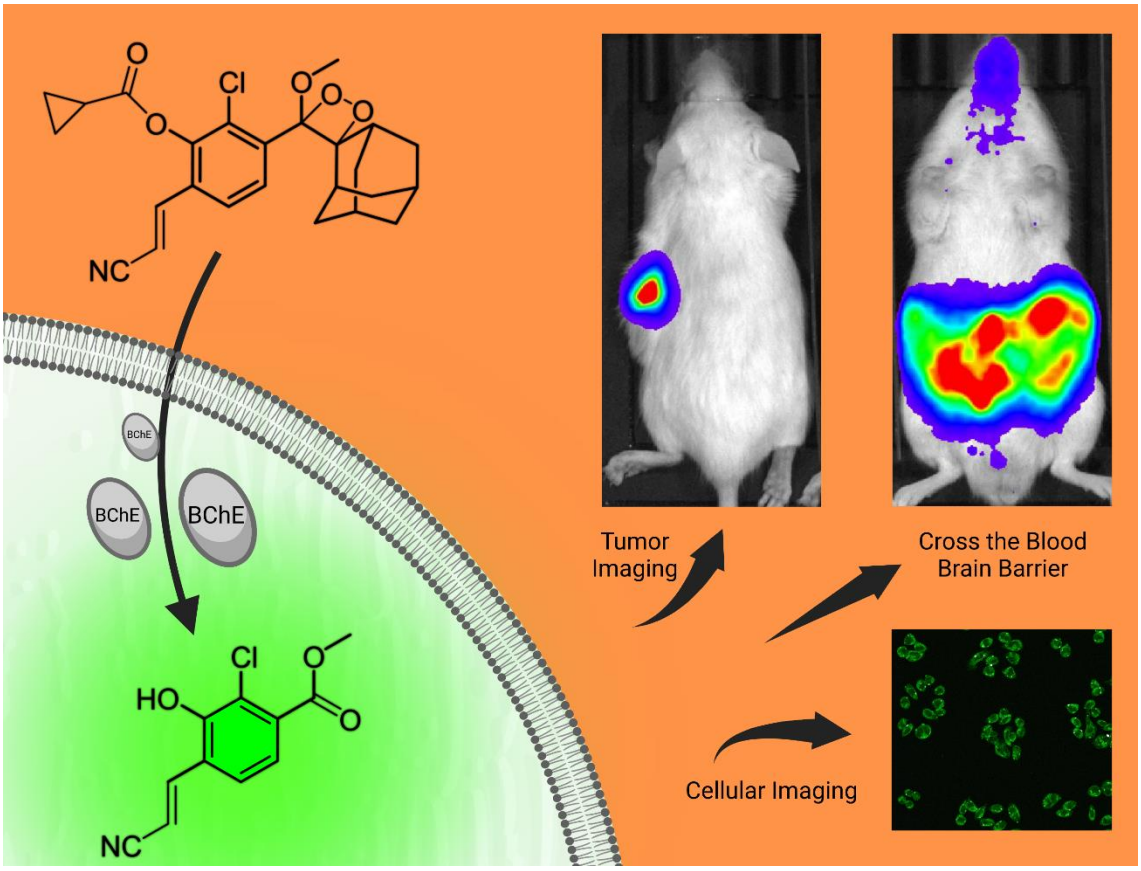

Figure 1.6: Applications of the BCC

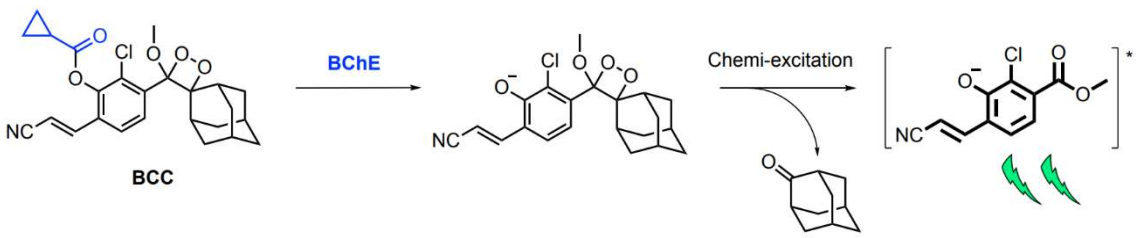

Figure 1.7: The design of the BCC

Chapter 2:
MATERIALS AND METHODS

2.1 Material and Instruments

Unless otherwise specified, all commercially available reagents were utilized without any additional purification. Butyrylcholinesterase from horse serum (C7512) and 9-Amino-1,2,3,4-tetrahydroacridine hydrochloride hydrate (Tacrine – A79922) were purchased from Sigma-Aldrich. The 4 Å molecular sieve was used to obtain anhydrous solvents. The Mbraun MBSPS5 solvent drying system was used for obtaining anhydrous THF. Argon was used to create an inert atmosphere. The ^{1}H NMR and ^{13}C NMR spectra were acquired at room temperature using a Bruker Avance III Ultrashield (500 MHz) spectrometer, with $CDCl_3$ as the solvent and tetramethylsilane (TMS) as the internal standard. The coupling constants (J values) are expressed in Hz, and the chemical shifts are reported in parts per million (ppm). Splitting patterns are as s (singlet), d (doublet), t (triplet), q (quartet), and m (multiplet). The MestReNova program was used to process the NMR spectra. Thick-walled glass columns filled with silica gel 60 (Merck 230-400 mesh) were used for column chromatography. Thin layer chromatography (TLC) was carried out using commercially available silica gel plates (Merck Silica Gel 60 F254) with a thickness of 0.25 mm. Visualization was performed under UV lamps. Mass analyses were performed with the Waters Vion QTOF mass spectrometer. Fluorescence spectra were acquired on the Agilent Cary Eclipse spectrophotometer. When referring to chromatography solvent mixtures, the relative proportions of solvents are expressed as volume-to-volume ratios.

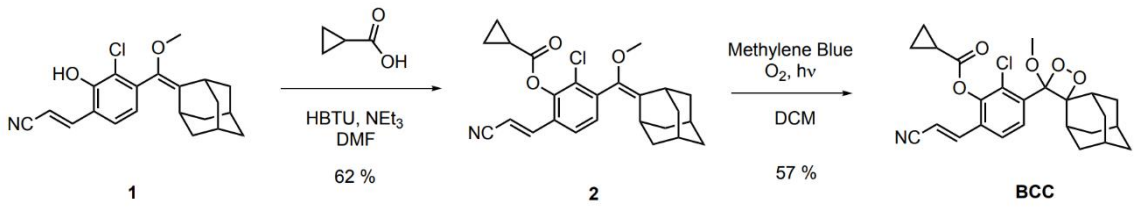

Scheme 2.1: Synthesis of BCC.

2.2 Synthesis

2.2.1 Synthesis of Compound 2

Triethylamine (134 µL, 0.955 mmol) and cyclopropanecarboxylic acid (20 mg, 0.232 mmol) were dissolved in DMF (2 mL), while stirring at room temperature under N_2. Next, HBTU (113 mg, 0.298 mmol) was portion-wise added, and it was stirred for half an hour. Consequently, compound 1 (68 mg, 0.191 mmol) was dissolved in DMF (2 mL) and added dropwise to the reaction mixture. It was stirred at room temperature overnight. Then, the reaction content was diluted with ethyl acetate (30 mL) and washed with brine and water. The organic layer was separated, and Na_2SO_4 was added to dry. Then, the mixture was concentrated under reduced pressure. The resulting crude product was purified through column chromatography on silica gel (Hex:EtOAc, 90:10). It isolated as a white solid (50 mg, 62 %). ^{1}H NMR (500 MHz, $CDCl_3$) δ 7.43 (s, 1H), 7.41 (d, J = 9.3 Hz, 1H), 7.21 (d, J = 8.1 Hz, 1H), 5.94 (d, J = 16.7 Hz, 1H), 3.30 (s, 3H), 3.27 (s, 1H), 2.07 (s, 1H), 1.97 – 1.64 (m, 13H), 1.29 (m, 2H), 1.18 – 1.13 (m, 2H). ^{13}C NMR (126 MHz, $CDCl_3$) δ 171.81, 145.85, 143.67, 138.97, 138.80, 133.45, 129.53, 129.51, 127.97, 124.01, 117.71, 99.50, 57.40, 39.22, 39.04, 38.59, 36.98, 32.91, 29.77, 28.29, 28.13, 12.76, 9.78. HRMS: m/z calculated for $C_{25}H_{26}ClNO_3Na$: 446.1499 $[M^+Na]^+$, found 446.1495.

2.2.2 Synthesis of BCC

Methylene Blue (2 mg, 0.006 mmol) was dissolved in O_2-bubbled DCM in the Schlenk tube. Next, compound 2 was transferred to the tube, and the reaction cooled to 0 °C. Next, the reaction mixture was continuously irradiated with a 595 nm LED light source for 2 hours while bubbling O_2 in the medium. Once the completion of the starting material was observed on TLC, the reaction mixture was concentrated again under reduced pressure. The resulting crude solid was purified through column chromatography on silica gel. (Hex:EtOAc, 95:5) to yield BCC (10.5 mg, 57 %). ^{1}H NMR (500 MHz, $CDCl_3$) δ 8.05 (d, J = 8.4 Hz, 1H), 7.57 (d, J = 8.4 Hz, 1H), 7.43 (d, J = 16.7 Hz, 1H), 6.02 (d, J = 16.8 Hz, 1H), 3.20 (s, 3H), 3.01 (s, 1H), 2.27 – 2.20 (m, 1H), 2.00 – 1.59 (m, 11H), 1.48 – 1.34 (m, 2H), 1.28 (dd, 2H), 1.19 – 1.14 (m, 2H). ^{13}C NMR (126 MHz, $CDCl_3$) δ 171.66, 146.50, 143.19, 136.26, 130.63, 129.83, 127.44, 124.21, 117.31,

111.46, 100.95, 96.41, 49.76, 39.28, 36.57, 33.91, 33.62, 32.17, 31.58, 26.17, 25.79, 12.69, 9.88, 9.76. HRMS: m/z calculated for $C_{25}H_{26}ClNO_5$: 455.1500 $[M]^+$, found 455.1521.

2.3 In solution Experiments

The BCC probe was dissolved in DMSO (5 mM), and the commercially available BChE enzyme was dissolved in dH_2O (240 U/ml) to prepare stock solutions. The stocks were aliquoted in small volumes and stored at -80 °C and -20 °C for BCC and BChE, respectively.

2.3.1 Measurement of Kinetic Fluorescence Spectra

To obtain kinetic fluorescence increase based on cage group cleavage, 10 µM BCC was treated with 20 U/ml BChE in a 3 mL cuvette (in DPBS, 1% DMSO). It was incubated at 37 °C throughout the process, and fluorescence spectra were recorded at 4-minute intervals by exciting the sample from 400 nm and collecting fluorescence from 430 – 700 nm (slit width 10/10). The data reported in the arbitrary unit (a.u.).

2.3.2 Analysis of HR-MS spectrum of BCC and The Resulting Benzoate

The corresponding analytes BCC and Benzoate resulting from the reaction between BCC and BChE were injected into Waters Vion QTOF mass spectrometer. The spectrum of 380 – 1000 Da and 230 - 1000 Da were obtained for BCC and resulting benzoate, respectively. The analytes were found at 455.15213 Da (BCC) and 238.02726 Da (Benzoate).

2.3.3 Detection of Time-dependent Chemiluminescence Intensity

96-well black-sided culture plates were used for the measurement. First, 50 µL various concentration BChE solutions (0-19.2 U/mL) were prepared by DPBS dilution, added into the wells of the plate, and incubated at 37 °C for 15 minutes. Then, 20 µM 50 µL BCC in DPBS (2% DMSO) was added into each well rapidly using a multichannel pipette, and the plate was shaken shortly. Overall, 10 µM BCC in DPBS (1% DMSO) was achieved as the final concentration in each well besides various BChE (0-19.2 U/mL). For the inhibition study, 19.2 U/mL BChE was incubated in the presence of 50 µM

Tacrine for 15 minutes prior to 10 µM BCC application. The kinetic luminescence measurements were acquired by Synergy H1 Reader (Biotek, USA) microplate reader at 37 °C for 2 hours without filter application. Each experiment was repeated three times.

2.3.4 Calculation of Detection limit

To calculate the detection limit, the formula 2.1 was used. The standard deviation (σ) of the chemiluminescent signal obtained from six separate BCC measurements (10 µM, 100 µL) was divided by the slope (k) of the enzymatic activity calibration curve obtained in step 1.3.3.

$$Detection\ limit\left(\frac{U}{mL}\right) = 3 * \frac{\sigma}{\mathrm{k}} \tag{2.1}$$

2.3.5 Evaluation of Inhibition Efficacy

The experiment was performed in 96-well black-sided culture plates. First, 50 µL 2.4 U/mL BChE in the presence of various concentrations of the Tacrine (0-1000 nM) was prepared by DPBS dilution (1% DMSO) and incubated at 37 °C for 15 minutes. Then, 20 µM 50 µL BCC in DPBS (2% DMSO) was added into each well rapidly using a multichannel pipette, and the plate was shaken shortly. The kinetic luminescence measurements were acquired by Synergy H1 Reader (Biotek, USA) microplate reader at 37 °C without filter application until peak luminescence was recorded. Each experiment was repeated three times. The inhibition efficiency was calculated at peak using the below formula where $I_{inhibited}$ is the luminescence intensity of the corresponding Tacrine inhibited group and $I_{uninhibited}$ is the control group.

$$Inhibition\ efficiency\ (\%) = \frac{|I_{uninhibited} - I_{inhibited}|}{I_{uninhibited}} * 100 \tag{2.2}$$

2.3.6 Evaluation of Kinetic Parameters K_m and k_{cat}

BCC titration was performed to calculate K_m and k_{cat} parameters. 96-well black-sided culture plates were used for the experiment. First, 50 µL 2.4 U/mL BChE solutions were prepared by DPBS dilution and incubated at 37 °C for 15 minutes. Then, 50 µL various concentrations of BCC (0-40 µM) in DPBS (2% DMSO) were added into each well rapidly using a multichannel pipette, and the plate was shaken shortly. The kinetic luminescence measurements were acquired by Synergy H1 Reader (Biotek, USA) microplate reader at 37 °C without filter application until peak luminescence was recorded. The K_m parameter was calculated at peak luminescence applying non-linear regression available in GraphPad software, which is based on the below formula where Y is the enzyme velocity, V_{max} is the maximum enzyme velocity, X is the substrate concentration and K_m is the Michaelis-Menten constant.

$$Y = \frac{V_{max} * X}{K_m + X} \tag{2.3}$$

The k_{cat} parameter was calculated at peak luminescence using GraphPad software based on the below formula where Y is the enzyme velocity, E_t is the concentration of enzyme catalytic sites, k_{cat} is the turnover number, X is the substrate concentration and K_m is the Michaelis-Menten constant.

$$Y = \frac{E_t * k_{cat} * X}{K_m + X} \tag{2.4}$$

2.3.7 Analysis of Selectivity

BCC's selectivity against other analytes like biothiols, ROS, ions, and enzymes was investigated. 50 µL of 2.4 U/mL BChE, 50 nM CES2, 10 U/mL AChE and Tyrosinase, 10 µg/mL MAOA and MAOB, 10 ng/ml LAP, 5 mM GSH and Cys, 100 µM H_2O_2, Mg^{2+}, Na^+, K^+, and SO_4^{2-} were treated with 10 µM 50 µL BCC (2% DMSO). The kinetic luminescence measurements were acquired by Synergy H1 Reader (Biotek, USA)

microplate reader at 37 °C without filter application until peak luminescence was recorded. The luminescence intensity at peak (9 minutes) was reported in a column graph form after normalizing all to the luminescence intensity of BChE.

2.4 In vitro Experiments

2.4.1 Cell Culture

HEK293T, HepG2, and SH-SY5Y cell lines were purchased from American Tissue Type Culture Collection (ACTT, USA). Cell Culture Media, Supplements, and Reagents were purchased from Gibco (USA). Cells were cultured in high glucose DMEM supplemented with 10% FBS and 1% Penicilin-Streptomycin antibiotics. Cells were passaged at 70% confluency using DPBS and Trypsin-EDTA (0.05%, phenol red). Cells were maintained in an Eppendorf Galaxy 170S incubator (humidified, 37 °C, 5% CO_2).

2.4.2 Analysis of Cell Viability

The Cell Titer-Glo® (CTG) Luminescent Cell Viability Assay was used to evaluate the viability of cells. The assay measures ATP levels based on the luciferase-luciferin reaction and indirectly determines the number of live cells. For the experiment, cells were seeded into 96-well black-sided culture plates ($1x10^4$ cells per well) and incubated overnight for proper attachment. The next day, various concentrations of BCC prepared in DMEM (1% DMSO) were applied to the cell for an hour, followed by fresh DMEM replacement. After 24 hours, subsequent to the initial BCC application, the old medium was replaced by the 1:10 mixture of CTG reagent and DMEM. The plate was shaken for 2 minutes and incubated for 8 minutes at room temperature. The luminescent signal was recorded using the Synergy H1 Reader (Biotek, USA) microplate reader without filter application. The survival of cells was expressed as the percentage of live cells in each sample compared to the DMSO control groups. Each experimental group was repeated three times.

2.4.3 Detection of Time-dependent Chemiluminescence Intensity

$1x10^4$ cells were seeded per well into the 96-well black-sided culture plates and incubated overnight for proper attachment. The next day, various concentrations of BCC

prepared in DPBS (1% DMSO) were applied to the cells, and the kinetic luminescence measurements were acquired by Synergy H1 Reader (Biotek, USA) microplate reader at 37 °C for 2 hours without filter application. For the inhibition studies, each cell line was incubated with 50 µM Tacrine in DMEM for an hour prior to 10 µM BCC application in DPBS (1% DMSO) and the kinetic luminescence measurement. The kinetic luminescence signal was reported as relative light units (RLU). The total luminescence signal was declared as the area under the curve (AUC, min x intensity). Each experimental group was repeated three times.

2.4.4 Evaluation of BCC activity through Confocal Microscopy

$2x10^4$ cells per dish were seeded into 35 mm glass bottom culture dishes for live cell confocal imaging, and the cells were incubated for two days to gain proper morphology. Cells were incubated with 10 µM BCC in DPBS (1% DMSO) for half an hour before microscopy. For the inhibition study, SH-SY5Y cells were incubated with 50 µM Tacrine in DMEM for an hour before 10 µM BCC application in DPBS (1% DMSO). All confocal studies were performed with DMI8 SP8 Inverted Confocal Microscope (Leica, Germany) at 40X magnification. The data were analyzed by LAS X software (Leica, Germany). The numerical data were obtained from a 50 µm to 50 µm square region of interest (ROI) filled with cells without space and reported as mean relative fluorescent intensity. Each experimental group has five unmatched images.

2.5 In vivo Experiments

The use of animals in the *in vivo* experiments was authorized by the institutional ethical committee of Koç University. Non-obese diabetic/severe combined immunodeficiency (NOD/SCID) mice that were 6-8 weeks old were utilized throughout the experiments. Mice were anesthetized with a continuous isoflurane-air mixture (1:1 ratio). The kinetic luminescence measurement was performed using IVIS Lumina Series III *in vivo* imaging instrument (Perkin Elmer, USA). The data was analyzed by IVIS Imaging Systems Living Image Software (Perkin Elmer, USA).

2.5.1 Investigation of in vivo imaging capabilities in mouse models

To understand if BCC is applicable for *in vivo* imaging of the internal organs and brain, healthy mice were injected with 100 µL 100 µM BCC (1% DMSO) intraperitoneally after being anesthetized. The kinetic luminescence measurement was started immediately prior to the injection and followed for half an hour. All experiments were repeated three times.

2.5.2 Investigation of in vivo imaging capabilities in tumor models

$2.5x10^6$ cells in 100 µL volume of DPBS were injected into the left flank area of the mouse with a 23-gauge needle. The tumor growth was followed via palpation. After the tumor diameter reached 0.3-0.5 cm size, 100 µL 100 µM BCC (1% DMSO) was injected intratumorally. The kinetic luminescence measurement was started immediately prior to the injection and followed for an hour. All experiments were repeated three times.

Chapter 3:
RESULT AND DISCUSSION

3.1 Synthesis

For the synthesis of BCC, compound (1) demonstrated in the Figure 3.1 was synthesized following a well-known protocol in the literature. Next, compound (1) was reacted with cyclopropanecarboxylic acid in the presence of HATU and triethylamine to form an ester (2). Ultimately, the synthesis of BCC was completed by reacting the ester (2) with singlet oxygen ($^1O_2$) produced in situ by irradiating methylene blue with a white LED light to create the 1,2-dioxetane bond. The overall yield of the BCC synthesis was calculated as 35%, and the product was characterized by 1H, 13C NMR, and HR-MS.

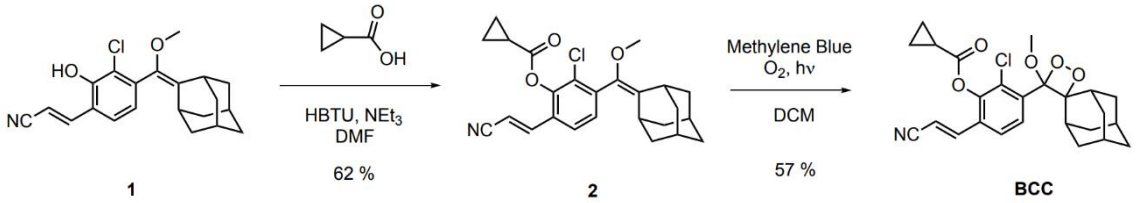

Scheme 3.1: Synthesis of BCC.

3.2 Optical Properties

After synthesizing the BBC probe, our second step was to analyze the fluorescence of the resulting benzoate created upon BChE-dependent enzymatic hydrolysis. To confirm if the enzyme could cleave the cyclopropyl cage unit, 10 µM BCC was treated with 20 U/mL BChE in pH 7.4 PBS solution containing 1% DMSO. A time-dependent increase in fluorescence signal was monitored in the spectrum that peaked at 525 nm, where benzoate has a characteristic signal[81] (Figure 3.2).

As predicted, the received fluorescence spectrum of the reaction-resulting benzoate excellently correlated with the previously reported literature data[81]. To further confirm the formation of benzoate upon the enzymatic activity, we conducted an HR-MS analysis with the reaction product of BCC and BChE. The detected a peak (238.0272 m/z) was consistent with the computed mass of the benzoate (238.0271 [M+H]+) (Figure 3.3).

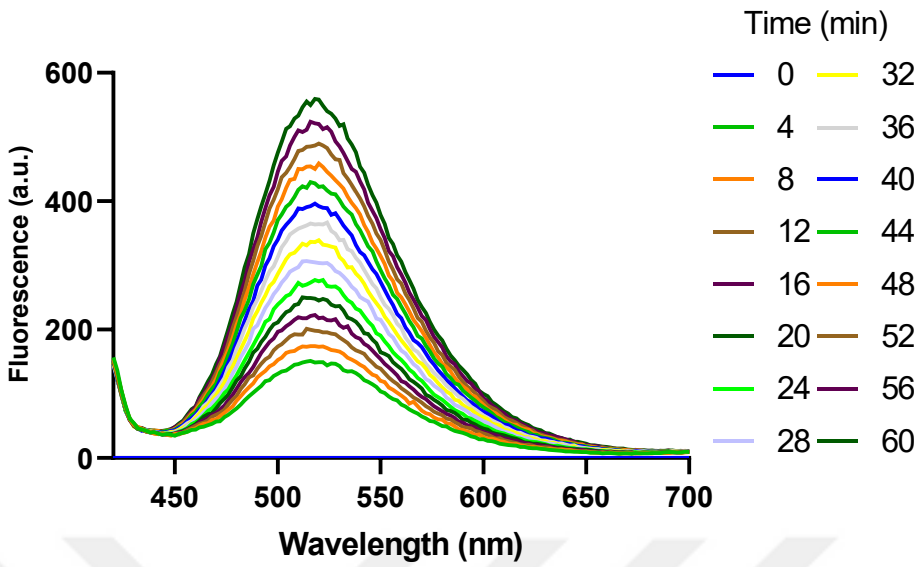

Figure 3.2: Fluorescence spectra upon treating BCC (10 µM) with a 20 U/mL BChE in PBS (1% DMSO, pH 7.4) (lex= 400 nm, width 10-10).

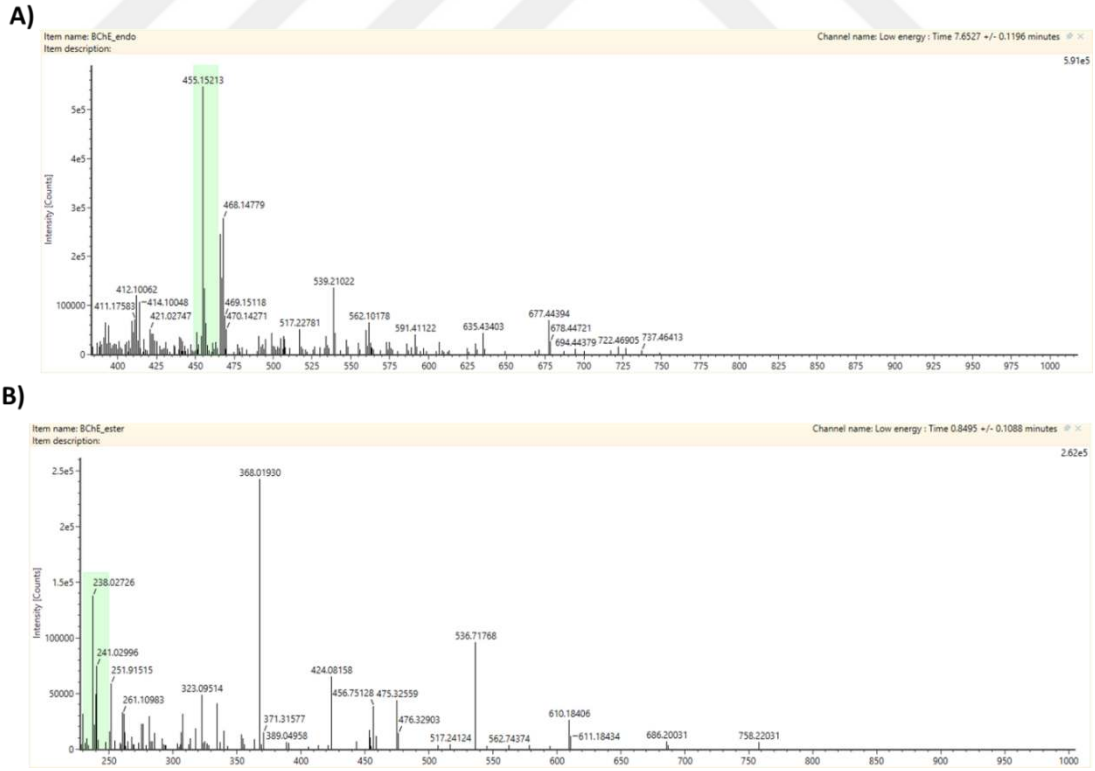

Figure 3.3: Mass Spectroscopy of (A) BCC and (B) Product (benzoate). Calculated at 238.02710, found at 238.02726.

3.3 Detection of the Chemiluminescence Signal

Following the encouraging results of the fluorescence studies, we investigated BCC's chemiluminescence response in pH 7.4 PBS solution containing 1% DMSO. 10 µM BCC was treated with increasing concentrations of BChE, ranging from 0 to 19.2 U/mL, and a dose-dependent increase was observed in the chemiluminescence signal for the first 10 minutes (Figure 3.4). After the initial 10-minute period, the chemiluminescent signal gradually decreased over two hours.

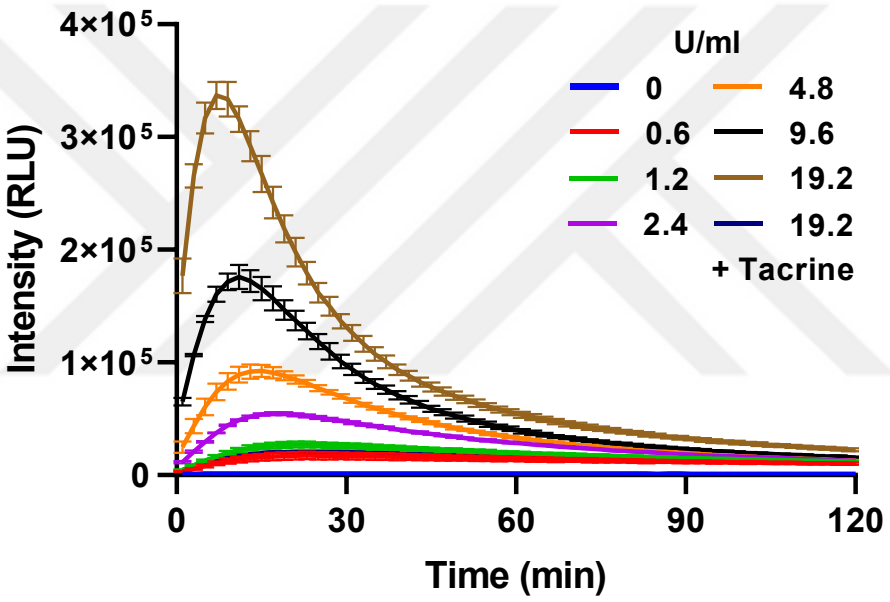

Figure 3.4: Time and BChE concentration dependent chemiluminescence intensity of BCC (10 µM) with and without of Tacrine (50 µM) in PBS (1% DMSO, pH 7.4). (n=3)

At the peak intensity, 19.2 U/mL BChE generated 570-fold more signal intensity than the control, showing negligible noise signal (Figure 3.5). Having no signal detection in the absence of the enzyme indicates that BCC is highly stable in aqueous solutions. This finding is significant as it demonstrates that the observed chemiluminescence response was due to the interaction between BCC and the enzyme rather than any instability or degradation of BCC in the solution.

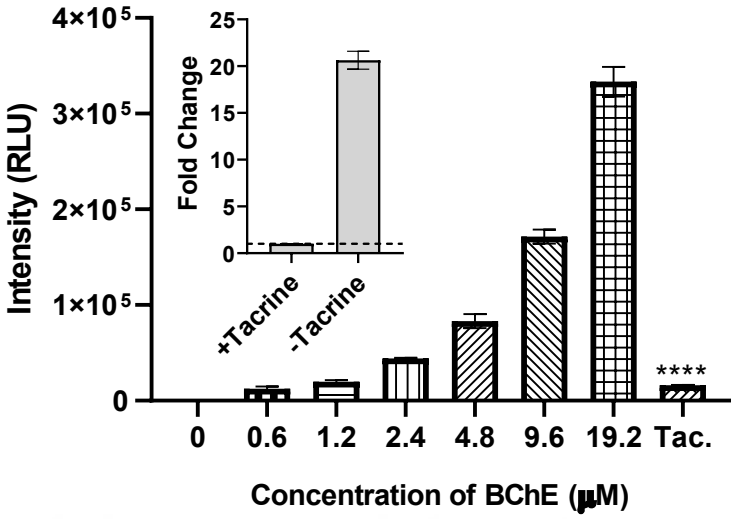

Figure 3.5: Maximum luminescence signal of BCC. Treated with increasing concentrations of BChE and Tacrine (50 µM) (at t=9 min). ($p<0,0001$). (n=3)

BCC's stability and high signal intensity are two significant indicators of a successful small molecule imaging probe. Still, the detection limit is a critical indicator of BCC's success. Therefore, a calibration curve with a linear fit (Figure 3.6) was created using the maximum luminescence data (Figure 3.5). Using the formula (2.1) and the slope of the calibration curve, the detection limit of BCC was calculated as 0.015 U/mL. It is lower than conventional BChE-responsive fluorophores' detection limits, summarized in Appendix A, highlighting that BCC is more sensitive and can detect lower BChE concentrations compared to alternative methods.

BChE was also treated with tacrine, a well-known inhibitor of BChE, as supplementary proof that BCC-related chemiluminescence is driven by BChE activity only. A significant decrease was observed in the intensity of the chemiluminescent signal when 19.2 U/ml BChE was treated with 50 µM tacrine for 15 minutes. The change between tacrine inhibition and control reached up to 20-fold, which firmly points out that the source of the chemiluminescence signal is the hydrolysis of BCC by BChE (Figure 3.4, 3.5).

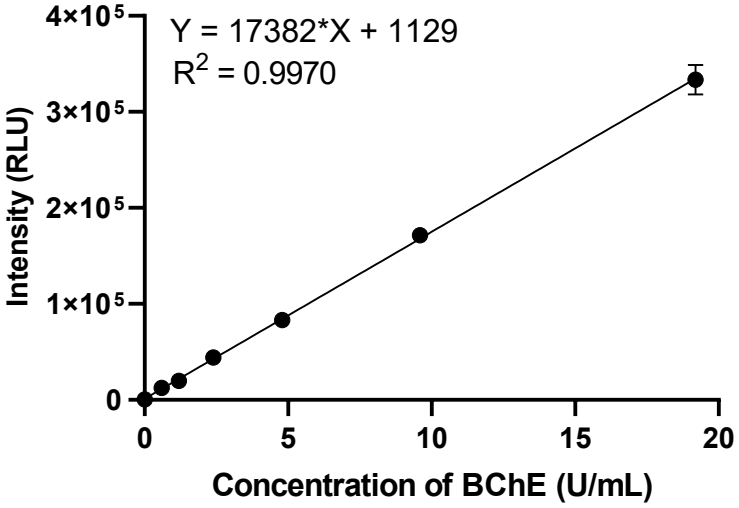

Figure 3.6: Calibration curve of the chemiluminescent signal intensity (at t=9 min). (n=3)

Tacrine inhibition of BChE and its effect on the hydrolysis of BCC was further investigated by titrating 2.4 U/mL BChE with increasing concentrations of tacrine in the presence of 10 µM BCC. It was encountered that increasing tacrine concentration enhanced the inhibition efficiency, which reached a plateau at 1 µM for 2.4 U/mL BChE (Figure 3.7). The inhibition coefficient (IC_{50}) was calculated as 25.04 nM (Table 1).

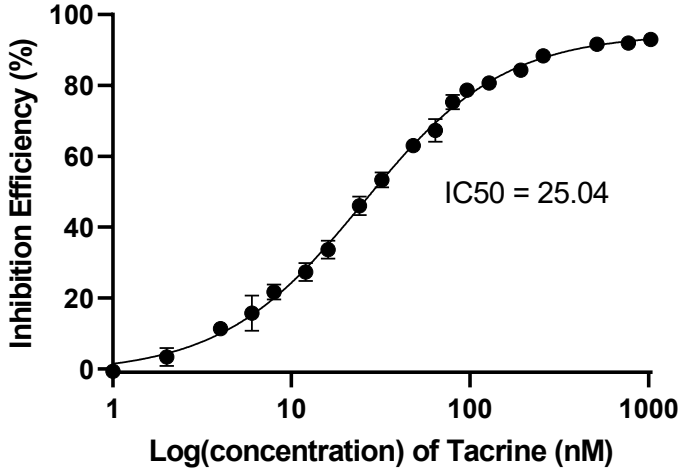

Figure 3.7: Tacrine concentration dependent inhibition of 2.4 U/mL BChE when treated with 10 µM BCC in PBS (1% DMSO, pH 7.4). (n=3)

To investigate the enzymatic activity in detail, BCC in various concentrations ranging from 0-40 µM was treated with 2.4 U/mL of BChE (Figure 3.8). A BCC concentration-dependent increase was acquired that plateaued at 40 µM. The results

depicted that the chemiluminescence intensity not only improves with increased concentration of BChE but also rises with increased concentration of BCC. The data were used to calculate the kinetic parameters K_m and k_{cat} using formulas (2.3) and (2.4), and respectively 3.7 µM and 8.615 sec^{-1} were found as K_m and k_{cat} (Table 1).

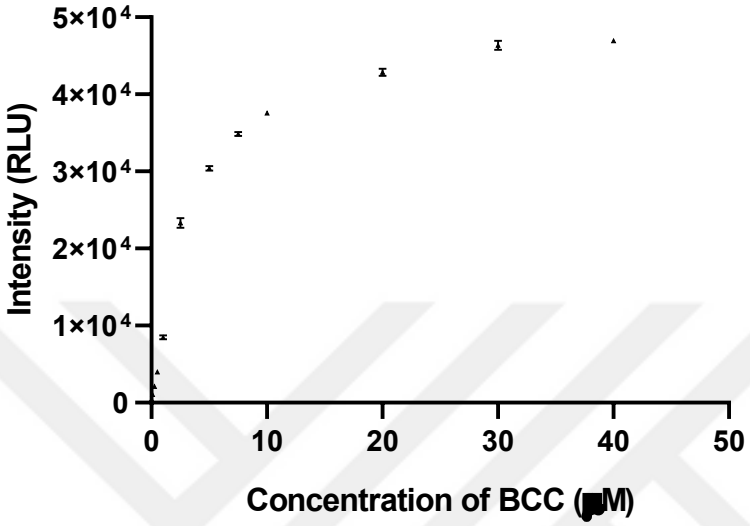

Figure 3.8: BCC concentration dependent chemiluminescence signal in the presence of BChE (2.4 U/ml) in PBS (1% DMSO, pH 7.4). (n=3)

Table 3.1: Enzyme kinetic and inhibition parameters

	K_m (µM)	k_{cat} (s^{-1})	k_{cat}/K_m ($µM^{-1}.s^{-1}$)	Tacrine IC_{50} (nM)
BCC	3.7	8.615	2.3	25.04

Besides its sensitivity, BCC was found to be highly selective towards BChE. In the selectivity assay, BCC was treated with several enzymes (BChE, CES2, AChE, Tyrosinase, MAOA, MAOB, LAP), biothiols (GSH and Cys), ROS (H_2O_2), and ions (Mg^{2+}, Zn^{2+}, Na^+, K^+, SO_4^{2-}). No significant chemiluminescence signal was detected from other analytes, indicating that BCC can be used as a reliable tool for the specific detection and measurement of BChE activity in complex biological environments without interference from other biomolecules (Figure 3.9). The signal obtained from AChE differentiated from others as being detectable. It was an expected noise because of the complex relationship between BChE and AChE, yet AChE-related noise is far from being adequate to deflect BCC's BChE selectivity.

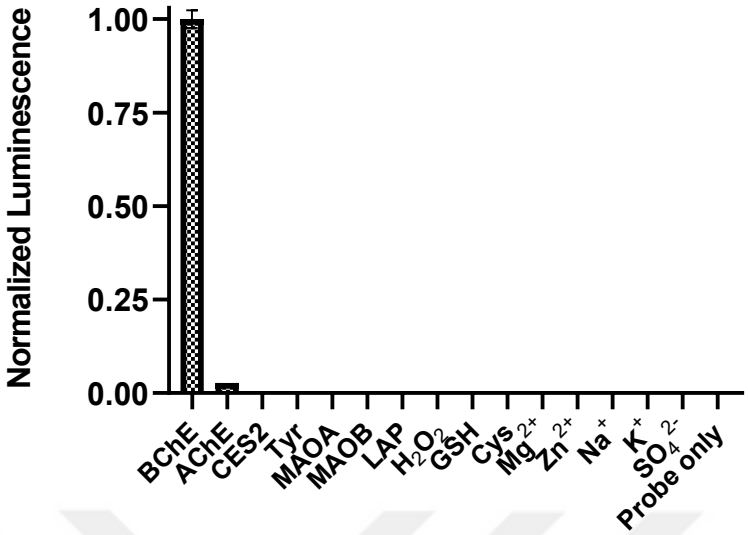

Figure 3.9: Luminescence signal of BCC with various enzymes and analytes (BChE at 2.4 U/ml, CES2 at 50 nM, AChE and Tyrosinase at 10 U/ml, MAOA and MAOB at 10 µg/ml, LAP at 10 ng/ml, GSH and Cys at 5 mM, others at 100 µM concentration). (n=3).

3.4 Imaging BChE Activity in Live Cells

After acquiring promising results with BCC *in solution*, we moved to test its ability to monitor endogenous BChE activity in human cell culture. HEK293T (non-cancerous), SH-SY5Y (neuroblastoma), and HepG2 (liver cancer) cell lines were chosen in this direction as diverse models. Before conducting visualization experiments, we checked BCC's cytotoxicity by treating all cell lines with increasing concentrations of BCC, ranging from 0.5-20 µM (Figures 3.10, 3.11, 3.12). No decline in cell viability was observed within the operating range; therefore, the BCC is safe for bioimaging in the living environment.

Upon seeing no toxicity in the cellular environment, BCC's *in vitro* detection capacity became the new target. The concentration- and time-dependent luminescence responses were investigated in all three cell lines (Figures 3.13, 3.14, 3.15, 3.19, 3.20). They were treated with varying concentrations of BCC ranging from 0-10 µM, and the chemiluminescence signal was collected for 2 hours. A rapid increase was monitored, reaching its peak value at 45 minutes, and then then the signal gradually decreased. A higher signal intensity was observed in the cancerous cell lines compared to HEK293T.

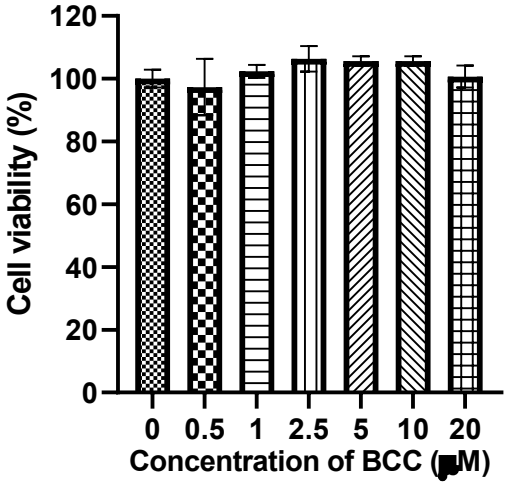

Figure 3.10: HEK293T Viability by CTG Assay. (n=3).

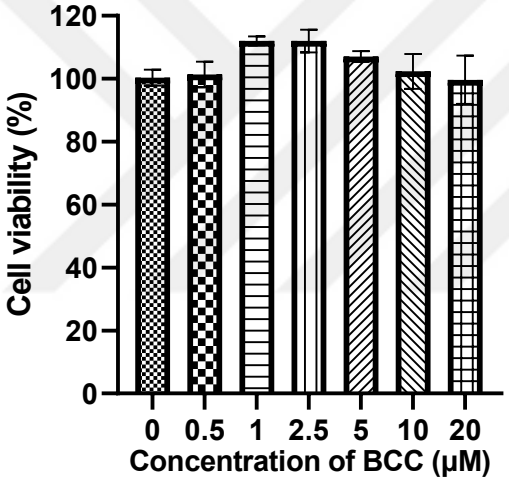

Figure 3.11: HepG2 Viability by CTG Assay. (n=3).

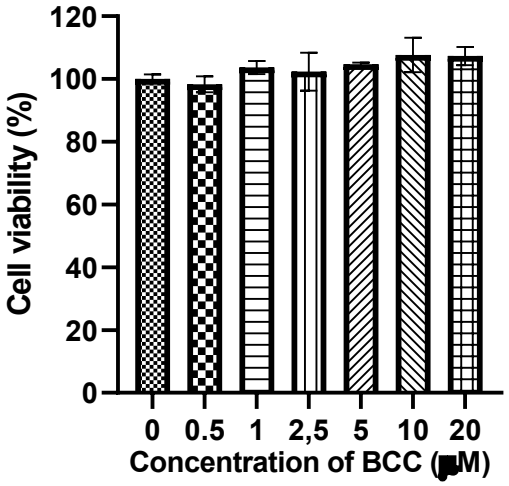

Figure 3.12: SH-SY5Y Viability by CTG Assay. (n=3).

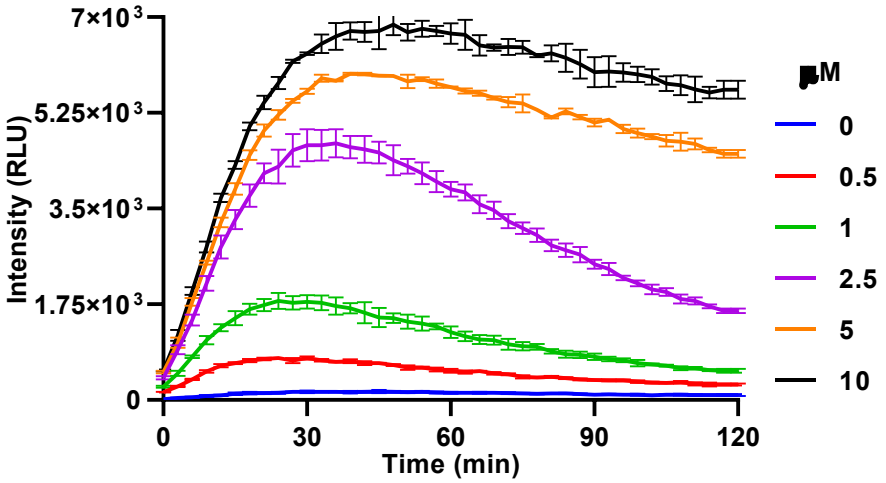

Figure 3.13: Time and dose dependent chemiluminescence signal of BCC in HEK293T.

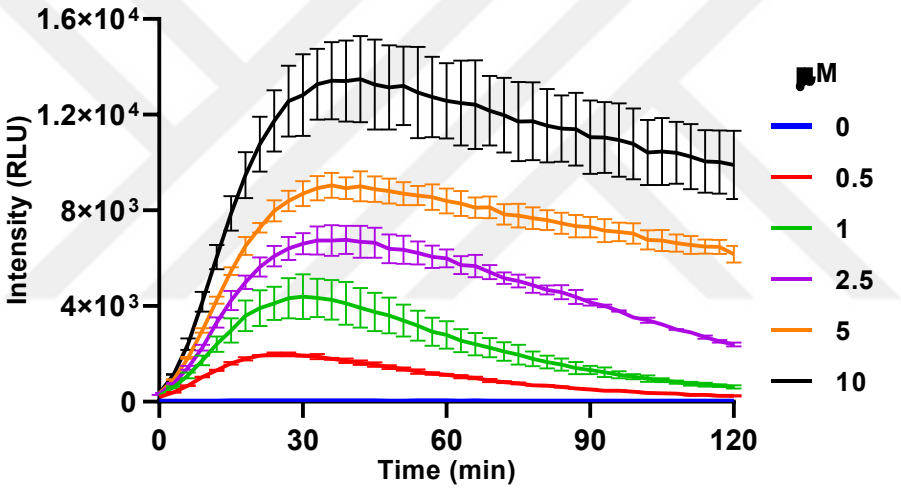

Figure 3.14: Time and dose dependent chemiluminescence signal of BCC in HepG2.

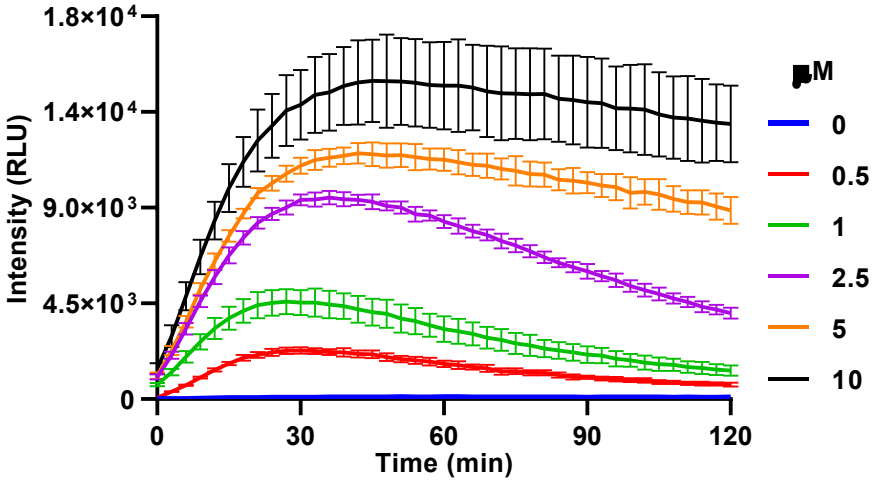

Figure 3.15: Time and dose dependent chemiluminescence signal of BCC in SH-SY5Y.

To confirm that signals were generated from endogenous BChE activity, we treated the cells with 50 µM tacrine for an hour and found that the chemiluminescence intensity significantly decreased in all three cell lines (Figures 3.16, 3.17, 3.18, 3.19, 3.20).

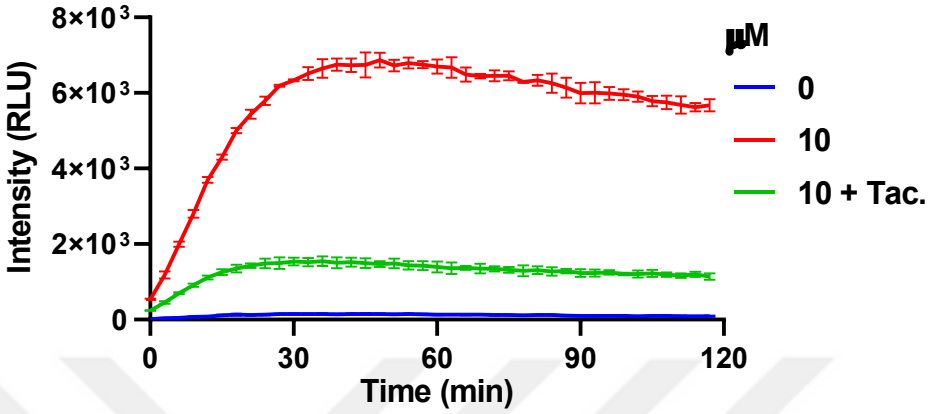

Figure 3.16: Time-dependent Tacrine (50 µM, 1h) inhibition in HEK293T. (n=3).

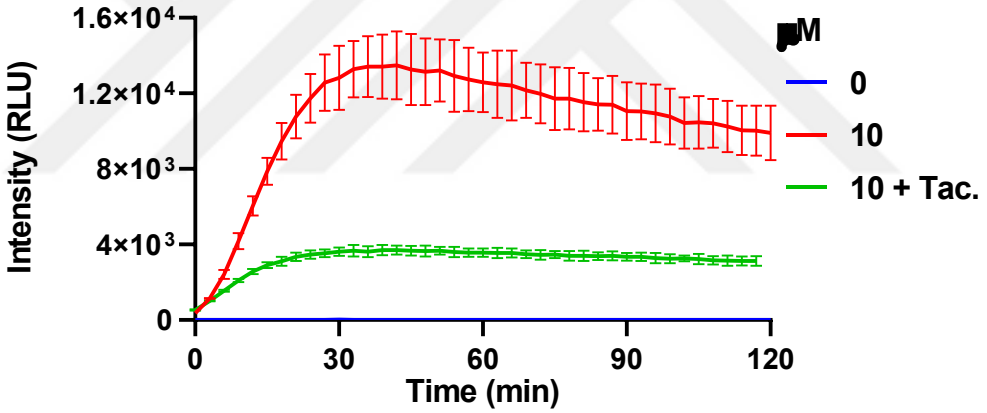

Figure 3.17: Time-dependent Tacrine (50 µM, 1h) inhibition in HepG2. (n=3).

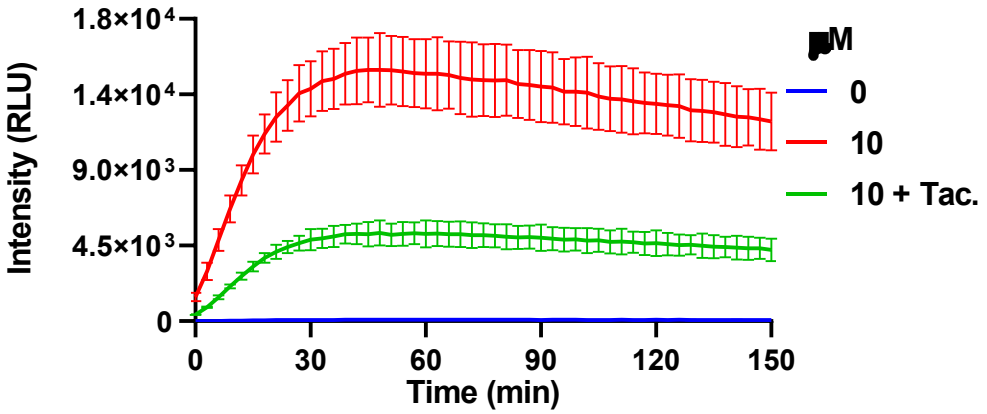

Figure 3.18: Time-dependent Tacrine (50 µM, 1h) inhibition in SH-SY5Y. (n=3).

Then, the total luminescent signal was found by calculating the areas under each curve (Figure 3.20). There was a linearity in the total luminescence in each curve up to 5 µM BCC treatment, showing that signal/BBC ratio is constant for different environments having different BChE concentration. Overall, the results of *in vitro* studies were in good correlation with the in-solution studies. Thus, it is proven that BCC is useful for detecting varying concentrations of BChE in the cellular environment, and the endogenous BChE activity is the primary source of the observed chemiluminescence signals.

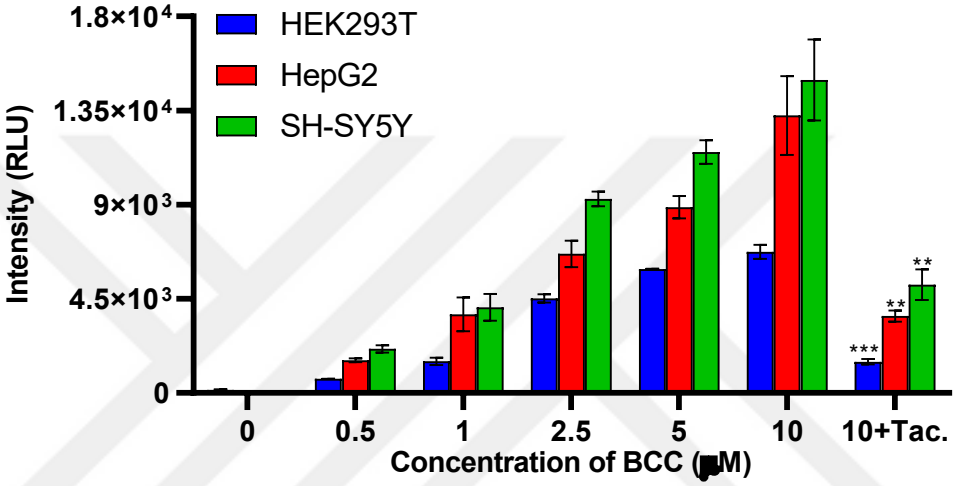

Figure 3.19: Maximum chemiluminescence signal of BCC after treating cells with increasing concentrations (at t=45 min). (n=3).

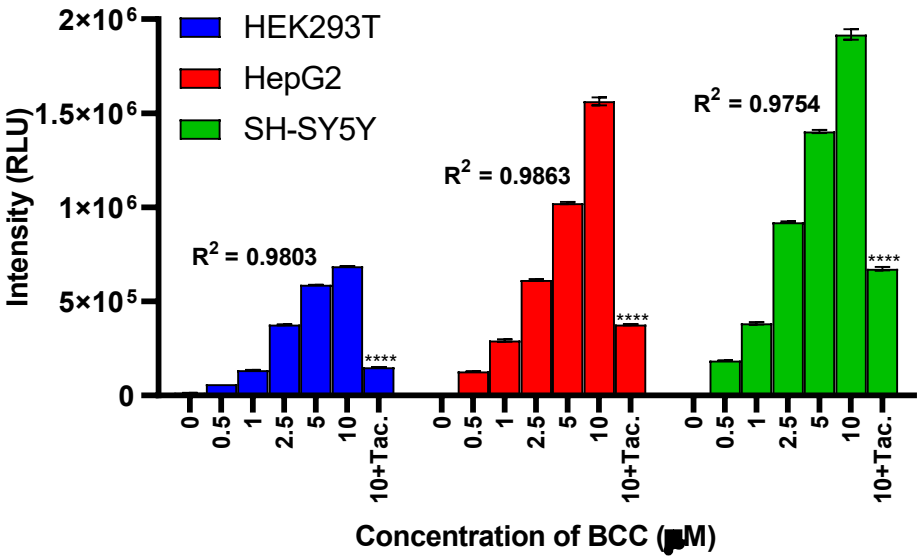

Figure 3.20: Total luminescent signal of BCC in 2 hours (AUC). R^2 value was calculated for the linear range between 0-5 µM. (n=3).

The imaging ability of BCC was further evaluated under confocal microscopy. To this end, HEK293T, HepG2, and SH-SY5Y cells were treated with 10 µM BCC for 2 hours. After the washing steps, the fluorescence of the resulting benzoate was observed by irradiating the cells with a 405 nm laser under confocal microscopy (Figure 3.21).

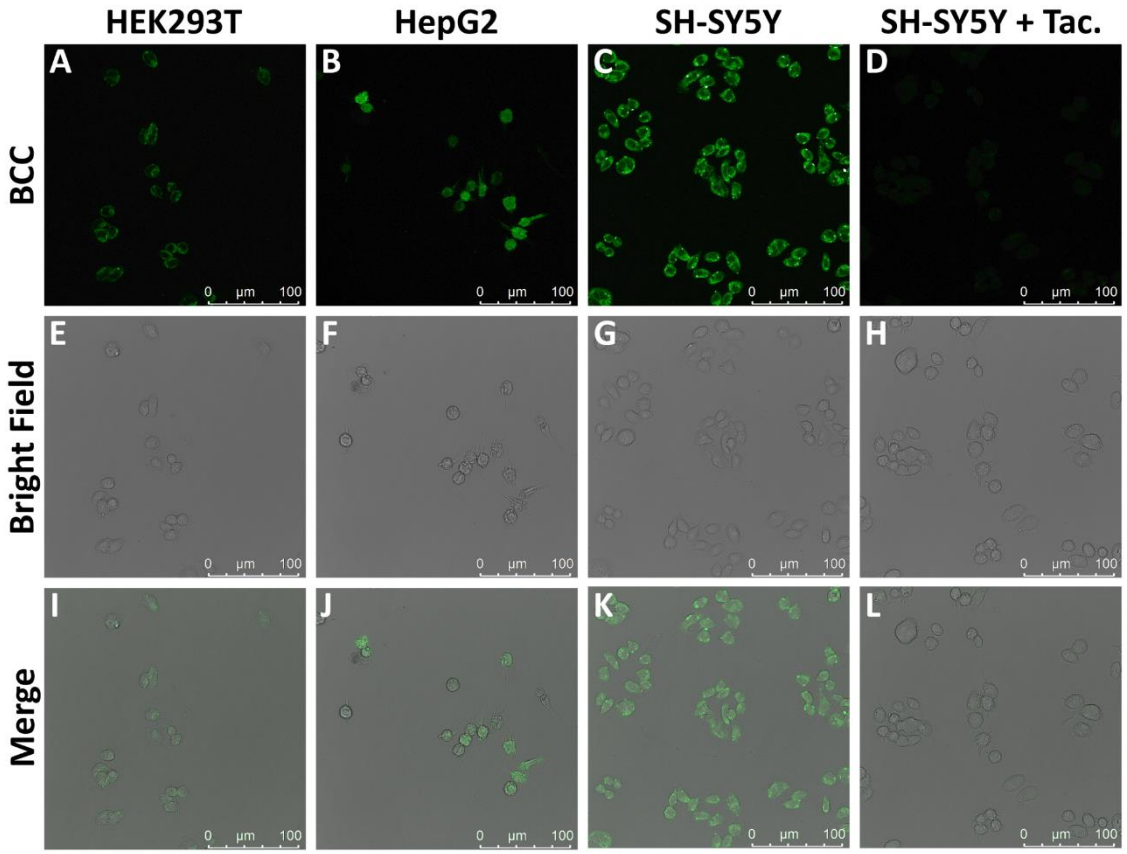

Figure 3.21: Confocal microscopy images of live (A,E,I) HEK293T, (B,F,J) HepG2 and (C,G,K) SH-SY5Y cells treated BCC (10 µM) for 2 hours. (D,H,L) SH-SY5Y cells pre-treated with Tacrine (50 µM) for 1 hour before BCC (10 µM) treatment for 2 hours. λ_{ex}= 405 nm / λ_{em}= 500-600 nm. Scale bar: 100µM.

The typical green emission of the benzoate was monitored at 525 nm. The signal intensity was higher in cancerous cell lines, consistent with the previous chemiluminescence measurements in the plate reader (Figure 3.22). In the inhibition study performed with 50 µM tacrine in SH-SY5Y cells, the fluorescence of the benzoate was quenched almost entirely and became virtually invisible, indicating that BCC could not be activated in the presence of the tacrine once more.

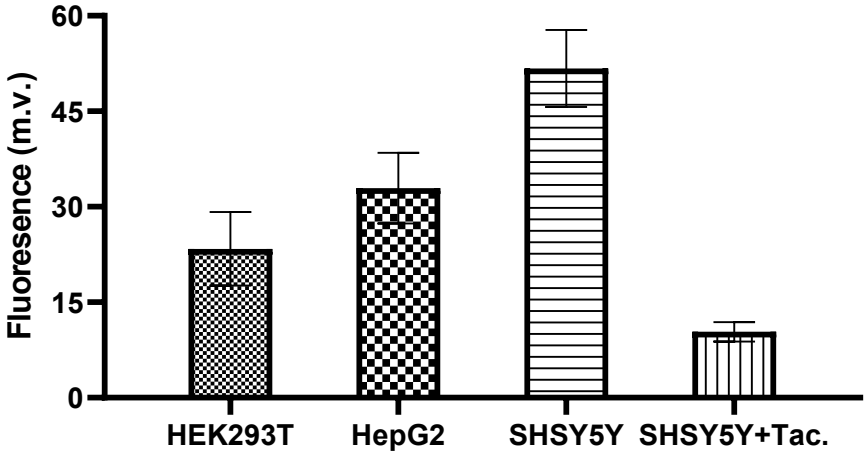

Figure 3.22: The fluorescence intensities of cells after 2 hours incubation with BCC (10 μM). (n=3).

In the time-dependent study, confocal images of BCC-treated SH-SY5Y cells showed that the probe starts emitting a considerable amount of light after 40 minutes of incubation (Figure 3.23, 3.25). Yet, the significant signal was detected after an hour.

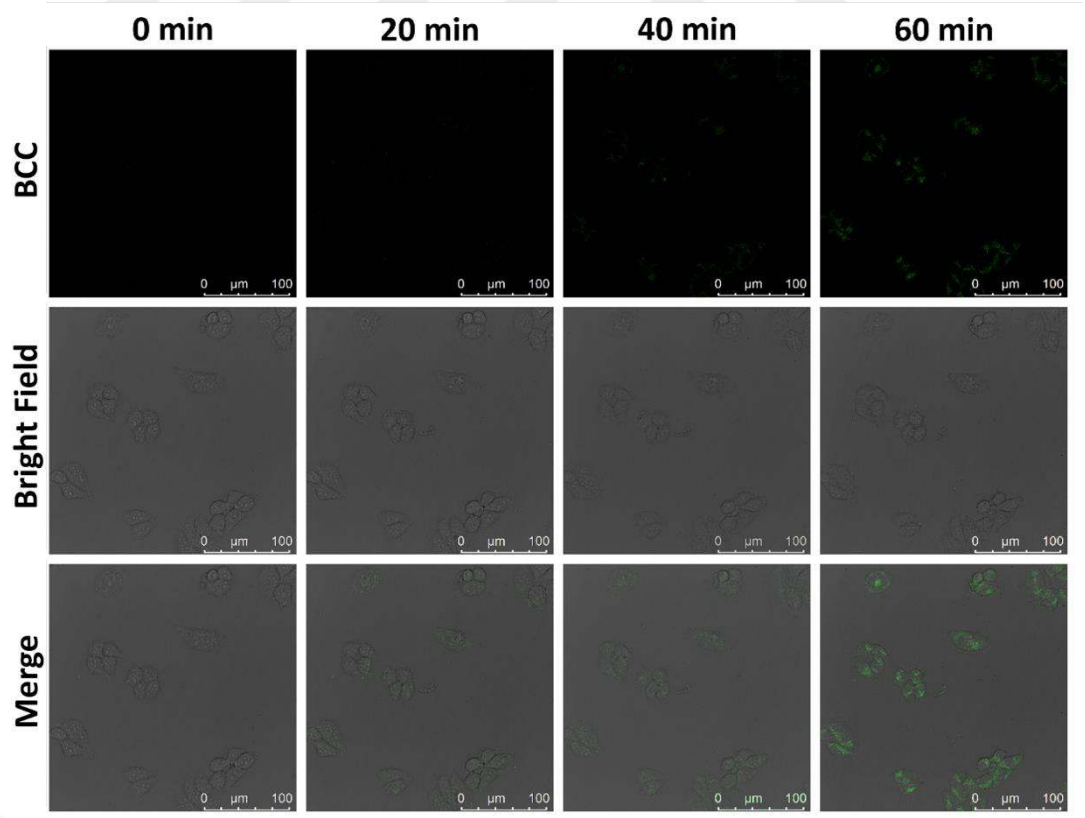

Figure 3.23: Time-dependent confocal images of SH-SY5Y cells that treated with BCC (10 μM)

A following time-dependent inhibition study further proved that chemiluminescent signal generation is prevented when BChE stays inactive throughout time (Figure 3.24, 3.25). Unfortunately, a BChE recover could not be observed through inhibition studies although tacrine is a reversable inhibitor.

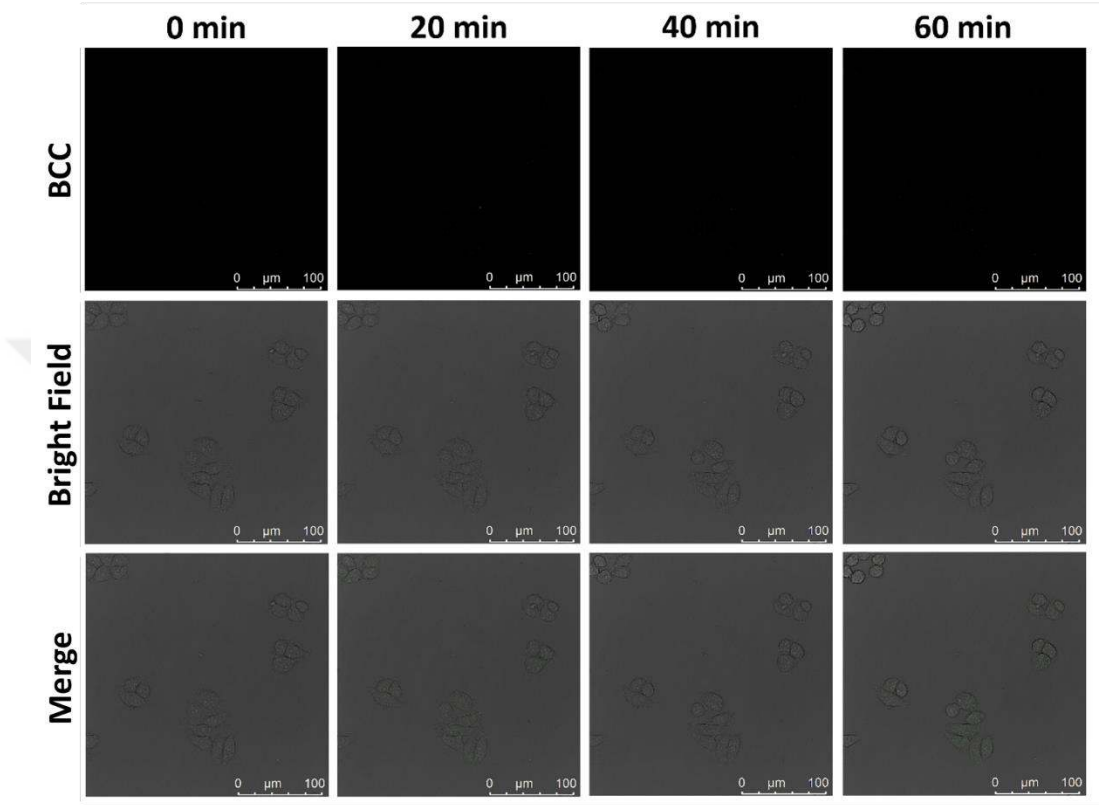

Figure 3.24: Time-dependent confocal images of SH-SY5Y cells that treated with BCC (10 µM) with prior Tacrine (50 µM) incubation for 1 hour.

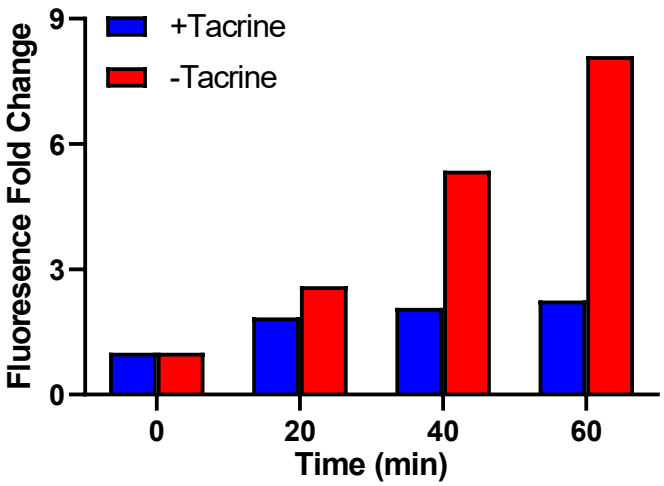

Figure 3.25: Fold change of fluorescence signal with and without Tacrine.

3.5 In vivo Imaging

We finally demonstrated BCC's capacity to conduct *in vivo* imaging in healthy and tumor-bearing mice models. First, BCC was intraperitoneally (IP) injected into healthy male mice to monitor the physiological BChE activity and followed through time (Figure 3.26). The intensity of the chemiluminescence signal increased rapidly and spread in the abdominal region, where organs such as the liver, kidneys, and prostate are located (Figure 3.26, 3.28). All these organs are known to have an enriched concentration of BChE, and the red spots seen in Figure 3.26 imply that the source of the signal is probably the organs themselves. In the control studies, no luminescence was detected when mice were injected with PBS.

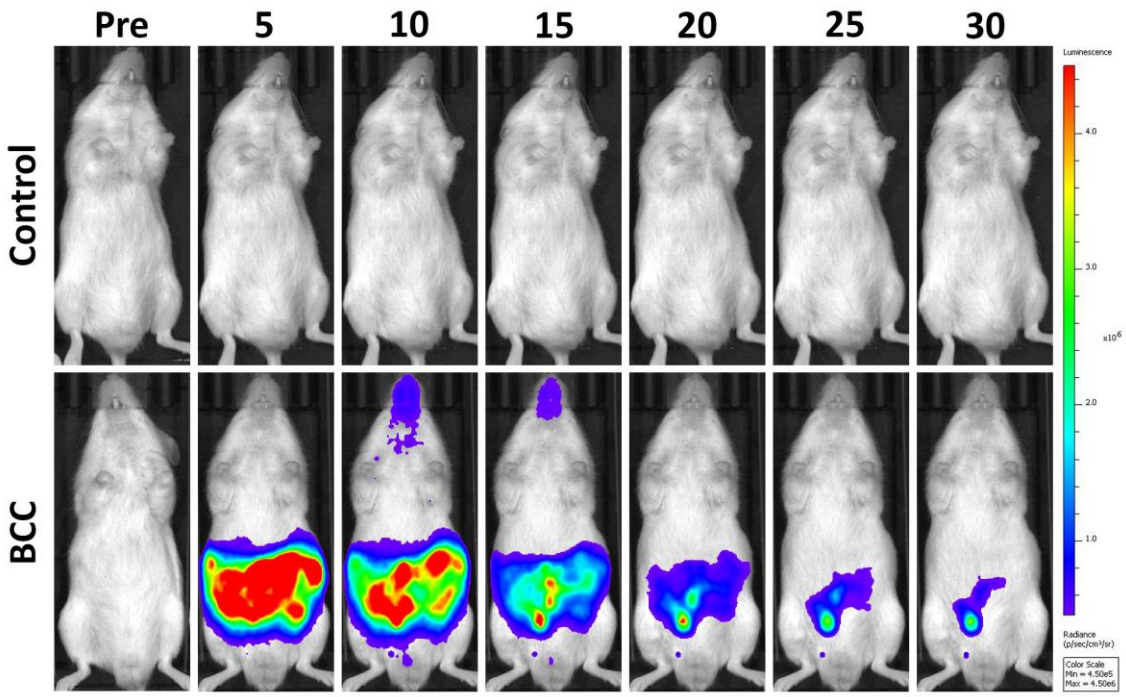

Figure 3.26: Time-dependent *in vivo* imaging of healthy mouse after intraperitoneal injection of PBS (top) (100 µL) or BCC (bottom) (100 µM, 100 µL). Time unit is minutes.

Notably, an outstanding signal was detected in the brain region, suggesting that BCC can penetrate the blood-brain barrier (BBB) and allows us to monitor intracerebral BChE activity (Figure 3.26, 3.27). The visualization of the brain took additional time since the BCC had to reach the head of the animal through circulation. Moreover, the blood-brain barrier may prevent the passage of high concentrations of BCC, causing the detection of lower chemiluminescent signal intensities in the brain region compared to the abdominal area.

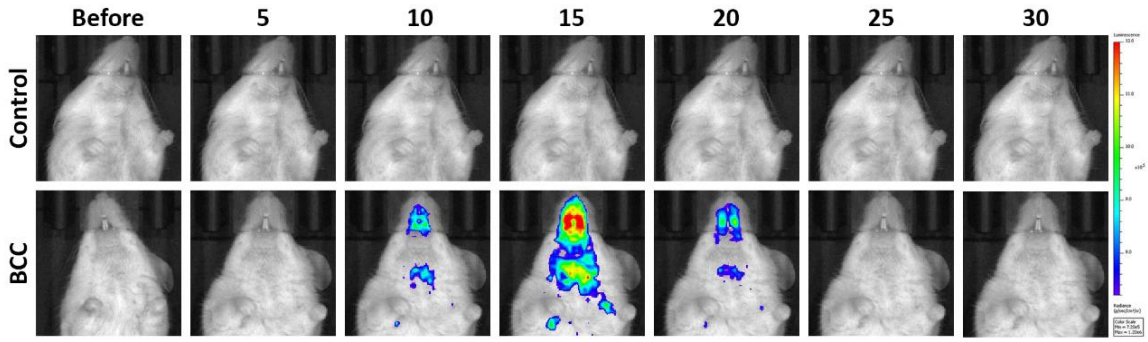

Figure 3.27: Time-dependent *in vivo* imaging of healthy mouse brain after intraperitoneal injection of PBS (top) (100 µL) or BCC (bottom) (100 µM, 100 µL). Time unit is minutes.

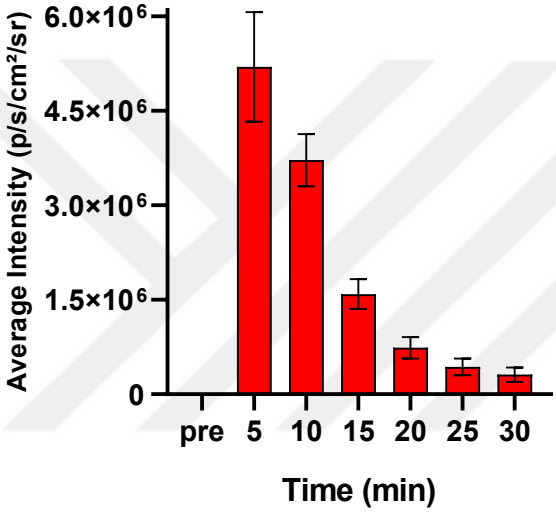

Figure 3.28: Time-dependent luminescence intensity in the abdominal region (n=3)

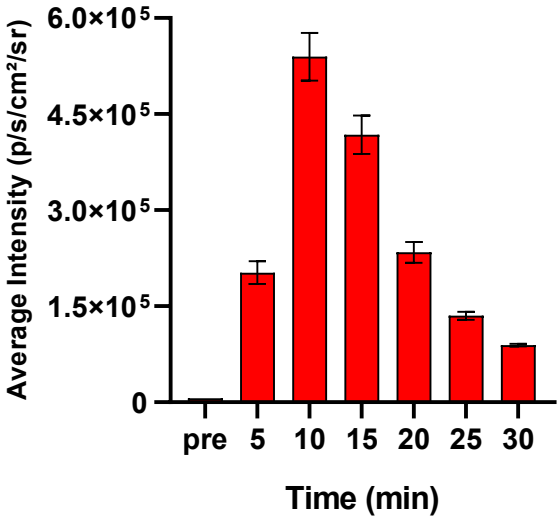

Figure 3.29: Time-dependent luminescence intensity in the brain region. (n=3).

The chemiluminescence signal decreased gradually within 30 minutes, and the remaining chemiluminescence signal accumulated in the bladder region. The flow of signal and the final accumulation area may speculate the removal of BCC through kidneys with time. Yet, no helpful information could be gathered from the urine of the animals about accumulated benzoate. Similarly, removing the organs after terminating animals did not give helpful information about the localization of BChE in organs because chemiluminescence provides real-time visualization and not an accumulated signal (Figure 3.30). But interestingly, there were still a detectable signal in the testicles.

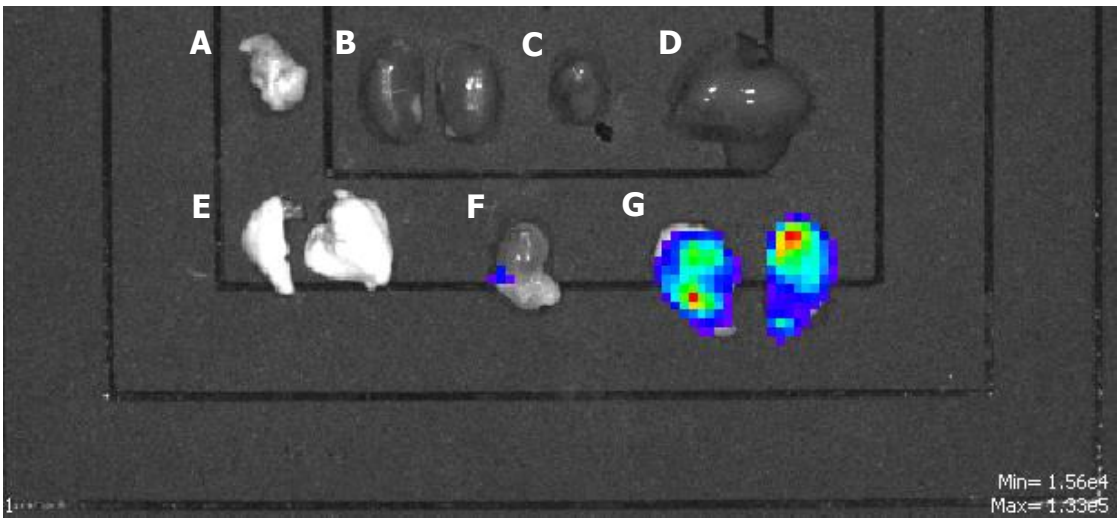

Figure 3.30: Chemiluminescent light intensities of major organs: A) Brain, B) Kidneys, C) Heart, D) Liver, E) Lung, F) Bladder, G) Testicles. The organs removed after termination of animals. (Signal unit = p/sec/cm^2/sr)

Later, SH-SY5Y cells were utilized to generate a tumor in immunocompromised mice models for investigating BChE activity *in vivo* tumor model. A time-dependent increase in chemiluminescent signal intensity was detected, reaching its peak at 25 minutes, and the intensity dropped gradually through time (Figure 3.31, 3.32).

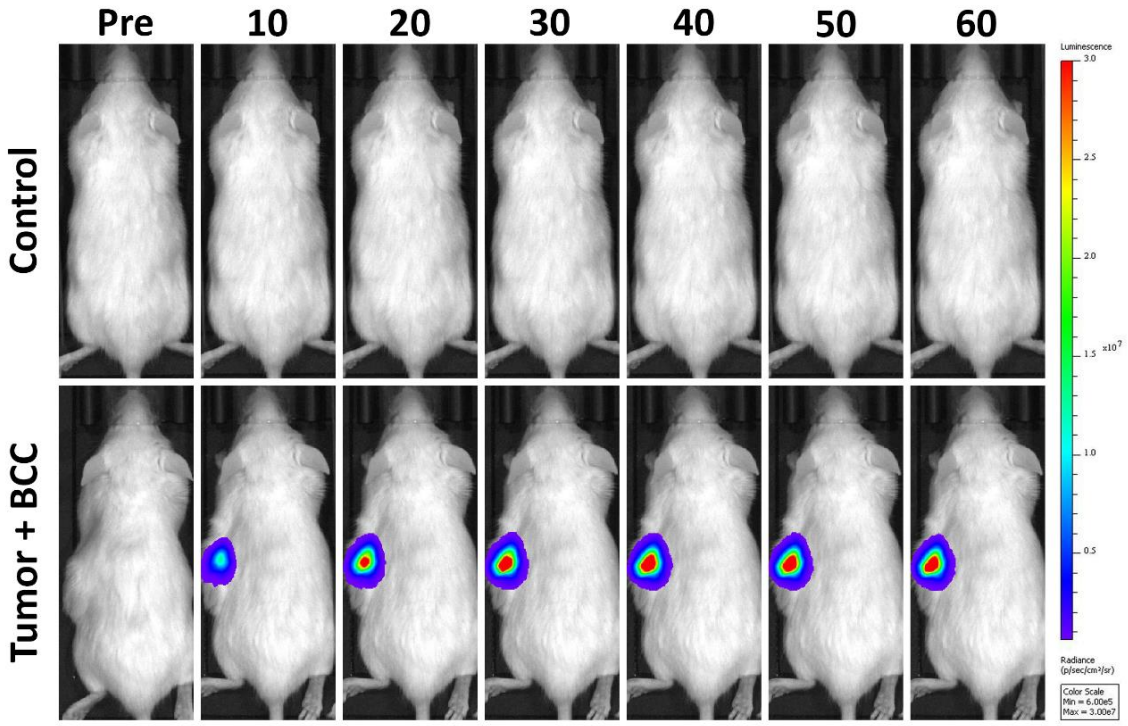

Figure 3.31: Time-dependent *in vivo* imaging of tumor bearing mice after subcutaneous injection of PBS (top) (100 µL) or intratumoral injection of BCC (bottom) (100 µM, 100 µL). Time unit is minutes.

However, BCC was found to be luminescent even after an hour. Like the healthy mice model, the injection of PBS did not trigger any chemiluminescence signal. One important notice is that BCC did not leak from the tumor region to interact with physiological BChE. It might be due to the hardness and low permeability of the tumor.

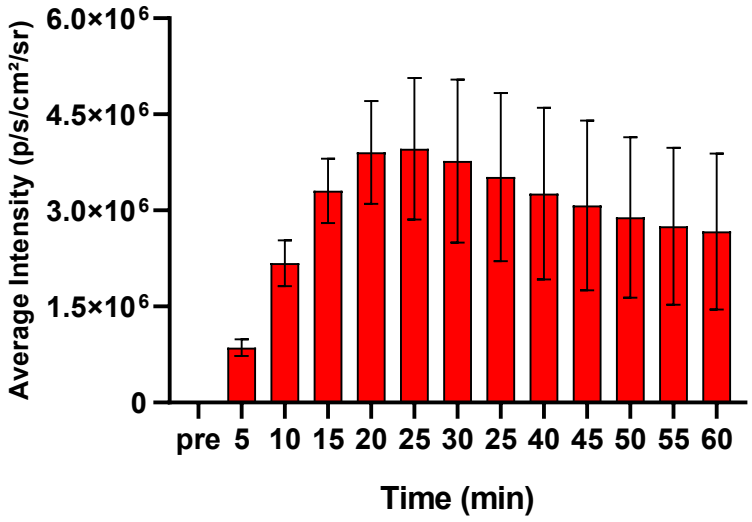

Figure 3.32: Time-dependent luminescence intensity in the tumor region (n=3).

Chapter 4:
CONCLUSION

To summarize, we have successfully developed a BChE-responsive chemiluminescent probe (BCC) based on a phenoxy 1,2-dioxetane core bearing an electron-withdrawing acrylic group. BCC demonstrated a significant turn-on response with BChE in aqueous solutions and generated an impressive chemiluminescent signal (570-fold) even in μM-level concentrations. It displayed remarkable stability at 37 C and exhibited selectivity only against BChE and not different analytes, including several enzymes, biothiols, ROS, and ions. BCC showed great sensitivity against BChE's concentration fluctuations while offering a low detection limit (0.015 U/mL). The BCC's chemiluminescent signal was inhibited completely with tacrine (20-fold). In cytotoxicity studies, BCC revealed no toxicity effect on healthy and cancerous cell lines treated with a broad concentration range. The probe was used to monitor endogenous BChE activity in HEK293T, HepG2, and SH-SY5Y cell lines, and a more powerful signal intensity was observed in cancerous cells compared to healthy cells. In vitro inhibition studies confirmed that the source of the signal is the reaction between BChE and the probe, meaning that their response can perform in the living environment without being affected by other intracellular processes. Later, BCC enabled us to visualize physiological BChE activity in healthy mice models. A rapid and robust signal was monitored in the abdominal region, which faded slowly in half an hour. BChE activity in the brain could be monitored thanks to BCC's ability to cross the blood-brain barrier. Additionally, BCC was utilized to image tumors generated by neuroblastoma cells on mouse models. Considering the contribution of BChE to physiological and pathological processes, it is essential to monitor BChE activity, changes in its concentration, and spatial/temporal distributions with high selectivity and sensitivity. With the promising results obtained here, we have acquired in this study, BCC can be further used to understand the unique roles of BChE in neurodegenerative diseases, psychiatric disorders, and drug resistance. Overall, our study has opened new avenues for real-time visualization of BChE for various biological and medical research and possesses the potential to use in clinical applications.

BIBLIOGRAPHY

(1) Lockridge, O. Review of Human Butyrylcholinesterase Structure, Function, Genetic Variants, History of Use in the Clinic, and Potential Therapeutic Uses. *Pharmacol. Ther.* **2015**, *148*, 34–46. https://doi.org/10.1016/j.pharmthera.2014.11.011.

(2) Johnson, G.; Moore, S. W. Why Has Butyrylcholinesterase Been Retained? Structural and Functional Diversification in a Duplicated Gene. *Neurochem. Int.* **2012**, *61* (5), 783–797. https://doi.org/10.1016/j.neuint.2012.06.016.

(3) Ha, Z. Y.; Mathew, S.; Yeong, K. Y. Butyrylcholinesterase: A Multifaceted Pharmacological Target and Tool. *Curr. Protein Pept. Sci.* **2019**, *21* (1), 99–109. https://doi.org/10.2174/1389203720666191107094949.

(4) Santarpia, L.; Grandone, I.; Contaldo, F.; Pasanisi, F. Butyrylcholinesterase as a Prognostic Marker: A Review of the Literature. *J. Cachexia. Sarcopenia Muscle* **2013**, *4* (1), 31–39. https://doi.org/10.1007/s13539-012-0083-5.

(5) Xing, S.; Li, Q.; Xiong, B.; Chen, Y.; Feng, F.; Liu, W.; Sun, H. Structure and Therapeutic Uses of Butyrylcholinesterase: Application in Detoxification, Alzheimer's Disease, and Fat Metabolism. *Med. Res. Rev.* **2021**, *41* (2), 858–901. https://doi.org/10.1002/med.21745.

(6) Johnson, G.; Moore, S. W. Why Has Butyrylcholinesterase Been Retained? Structural and Functional Diversification in a Duplicated Gene. *Neurochem. Int.* **2012**, *61* (5), 783–797. https://doi.org/10.1016/j.neuint.2012.06.016.

(7) Chatonnet, A.; Lockridge, O. Comparison of Butyrylcholinesterase and Acetylcholinesterase. *Biochem. J.* **1989**, *260* (3), 625–634. https://doi.org/10.1042/bj2600625.

(8) Davis, L.; Britten, J. J.; Morgan, M. Cholinesterase Its Significance in Anaesthetic Practice. *Anaesthesia* **1997**, *52* (3), 244–260. https://doi.org/10.1111/j.1365-2044.1997.084-az0080.x.

(9) WILSON, I. B.; HARRISON, M. A. Turnover Number of Acetyl-Cholinesterase. *J. Biol. Chem.* **1961**, *236*, 2292–2295.

(10) Randell, E. W.; Mathews, M. S.; Zhang, H.; Seraj, J. S.; Sun, G. Relationship between Serum Butyrylcholinesterase and the Metabolic Syndrome. *Clin. Biochem.* **2005**, *38* (9), 799–805.

https://doi.org/10.1016/j.clinbiochem.2005.04.008.

(11) Sridhar, G. R.; Rao, A. A.; Srinivas, K.; Nirmala, G.; Lakshmi, G.; Suryanarayna, D.; Nageswara Rao, P. V.; Kaladhar, D. G. S. V. G. L.; Kumar, S. V.; Devi, T. U.; Nitesh, T.; Hanuman, T. Butyrylcholinesterase in Metabolic Syndrome. *Med. Hypotheses* **2010**, *75* (6), 648–651. https://doi.org/10.1016/j.mehy.2010.08.008.

(12) Gilmer, J. F.; Lally, M. N.; Gardiner, P.; Dillon, G.; Gaynor, J. M.; Reidy, S. Novel Isosorbide-Based Substrates for Human Butyrylcholinesterase. *Chem. Biol. Interact.* **2005**, *157–158*, 317–319. https://doi.org/10.1016/j.cbi.2005.10.095.

(13) Sawatzky, E.; Al-Momani, E.; Kobayashi, R.; Higuchi, T.; Samnick, S.; Decker, M. A Novel Way To Radiolabel Human Butyrylcholinesterase for Positron Emission Tomography through Irreversible Transfer of the Radiolabeled Moiety. *ChemMedChem* **2016**, *11* (14), 1540–1550. https://doi.org/10.1002/cmdc.201600223.

(14) Yu, Z.; Li, X.; Lu, X.; Guo, Y. Rational Construction of a Novel Probe for the Rapid Detection of Butyrylcholinesterase Stress Changes in Apoptotic Cells. *New J. Chem.* **2022**, *46* (25), 12034–12040. https://doi.org/10.1039/D2NJ01678H.

(15) Evans, F. T.; Gray, P. W. S.; Lehmann, H.; Silk, E. Effect of Pseudo-Cholinesterase Level on Action of Succinylcholine in Man. *BMJ* **1953**, *1* (4802), 136–138. https://doi.org/10.1136/bmj.1.4802.136.

(16) Robles, A.; Michael, M.; McCallum, R. Pseudocholinesterase Deficiency: What the Proceduralist Needs to Know. *Am. J. Med. Sci.* **2019**, *357* (3), 263–267. https://doi.org/10.1016/j.amjms.2018.11.002.

(17) LEHMANN, H. THE FAMILIAL INCIDENCE OF LOW PSEUDOCHOLINESTERASE LEVEL. *Lancet* **1956**, *268* (6934), 124. https://doi.org/10.1016/S0140-6736(56)90869-8.

(18) Raveh, L.; Grunwald, J.; Marcus, D.; Papier, Y.; Cohen, E.; Ashani, Y. Human Butyrylcholinesterase as a General Prophylactic Antidote for Nerve Agent Toxicity. *Biochem. Pharmacol.* **1993**, *45* (12), 2465–2474. https://doi.org/10.1016/0006-2952(93)90228-O.

(19) Ahmed, M.; Rocha, J. B. T.; Mazzanti, C. M.; Morsch, A. L. B.; Cargnelutti, D.; Corrêa, M.; Loro, V.; Morsch, V. M.; Schetinger, M. R. C. Malathion,

Carbofuran and Paraquat Inhibit Bungarus Sindanus (Krait) Venom Acetylcholinesterase and Human Serum Butyrylcholinesterase in Vitro. *Ecotoxicology* **2007**, *16* (4), 363–369. https://doi.org/10.1007/s10646-007-0137-1.

(20) Gómez-Ramos, P.; Morán, M. A. Ultrastructural Localization of Butyrylcholinesterase in Senile Plaques in the Brains of Aged and Alzheimer Disease Patients. *Mol. Chem. Neuropathol.* **1997**, *30* (3), 161–173. https://doi.org/10.1007/BF02815095.

(21) Li, Q.; Yang, H.; Chen, Y.; Sun, H. Recent Progress in the Identification of Selective Butyrylcholinesterase Inhibitors for Alzheimer's Disease. *Eur. J. Med. Chem.* **2017**, *132*, 294–309. https://doi.org/10.1016/j.ejmech.2017.03.062.

(22) Ruberg, M.; Rieger, F.; Villageois, A.; Bonnet, A. M.; Agid, Y. Acetylcholinesterase and Butyrylcholinesterase in Frontal Cortex and Cerebrospinal Fluid of Demented and Non-Demented Patients with Parkinson's Disease. *Brain Res.* **1986**, *362* (1), 83–91. https://doi.org/10.1016/0006-8993(86)91401-0.

(23) Dong, M.-X.; Xu, X.-M.; Hu, L.; Liu, Y.; Huang, Y.-J.; Wei, Y.-D. Serum Butyrylcholinesterase Activity: A Biomarker for Parkinson's Disease and Related Dementia. *Biomed Res. Int.* **2017**, *2017*, 1–9. https://doi.org/10.1155/2017/1524107.

(24) Barbosa, M.; Rios, O.; Velásquez, M.; Villalobos, J.; Ehrmanns, J. Acetylcholinesterase and Butyrylcholinesterase Histochemical Activities and Tumor Cell Growth in Several Brain Tumors. *Surg. Neurol.* **2001**, *55* (2), 106–112. https://doi.org/10.1016/S0090-3019(01)00351-2.

(25) Gu, Y.; Chow, M. J.; Kapoor, A.; Mei, W.; Jiang, Y.; Yan, J.; De Melo, J.; Seliman, M.; Yang, H.; Cutz, J. C.; Bonert, M.; Major, P.; Tang, D. Biphasic Alteration of Butyrylcholinesterase (BChE) During Prostate Cancer Development. *Transl. Oncol.* **2018**, *11* (4), 1012–1022. https://doi.org/10.1016/j.tranon.2018.06.003.

(26) Prabhu, K.; Naik, D.; Ray, S.; Vadiraj; Rao, A.; Kamath, A. Significance of Serum Butyrylcholinesterase Levels in Oral Cancer. *Australas. Med. J.* **2011**, *4* (7), 374–378. https://doi.org/10.4066/AMJ.2011.569.

(27) Onder, S.; Schopfer, L. M.; Jiang, W.; Tacal, O.; Lockridge, O.

Butyrylcholinesterase in SH-SY5Y Human Neuroblastoma Cells. *Neurotoxicology* **2022**, *90* (January), 1–9. https://doi.org/10.1016/j.neuro.2022.02.006.

(28) Alcântara, V. M.; Chautard-Freire-Maia, E. A.; Scartezini, M.; Cerci, M. S. J.; Braun-Prado, K.; Picheth, G. Butyrylcholinesterase Activity and Risk Factors for Coronary Artery Disease. *Scand. J. Clin. Lab. Invest.* **2002**, *62* (5), 399–404. https://doi.org/10.1080/00365510260296564.

(29) Lampón, N.; Hermida-Cadahia, E. F.; Riveiro, A.; Tutor, J. C. Association between Butyrylcholinesterase Activity and Low-Grade Systemic Inflammation. *Ann. Hepatol.* **2012**, *11* (3), 356–363. https://doi.org/10.1016/S1665-2681(19)30932-9.

(30) Chen, V. P.; Gao, Y.; Geng, L.; Stout, M. B.; Jensen, M. D.; Brimijoin, S. Butyrylcholinesterase Deficiency Promotes Adipose Tissue Growth and Hepatic Lipid Accumulation in Male Mice on High-Fat Diet. *Endocrinology* **2016**, *157* (8), 3086–3095. https://doi.org/10.1210/en.2016-1166.

(31) Lanctôt, K. L.; Herrmann, N.; Yau, K. K.; Khan, L. R.; Liu, B. A.; LouLou, M. M.; Einarson, T. R. Efficacy and Safety of Cholinesterase Inhibitors in Alzheimer's Disease: A Meta-Analysis. *CMAJ* **2003**, *169* (6), 557–564.

(32) Tan, L. Efficacy and Safety of Donepezil, Galantamine, Rivastigmine, and Memantine for the Treatment of Alzheimer's Disease: A Systematic Review and Meta-Analysis. *J. Alzheimers. Dis.* **2014**, *41* (2), 615–631. https://doi.org/10.3233/JAD-132690.

(33) Hartmann, J.; Kiewert, C.; Duysen, E. G.; Lockridge, O.; Greig, N. H.; Klein, J. Excessive Hippocampal Acetylcholine Levels in Acetylcholinesterase-Deficient Mice Are Moderated by Butyrylcholinesterase Activity. *J. Neurochem.* **2007**, *100* (5), 1421–1429. https://doi.org/10.1111/j.1471-4159.2006.04347.x.

(34) Reid, G. A.; Darvesh, S. Butyrylcholinesterase-Knockout Reduces Brain Deposition of Fibrillar β-Amyloid in an Alzheimer Mouse Model. *Neuroscience* **2015**, *298*, 424–435. https://doi.org/10.1016/j.neuroscience.2015.04.039.

(35) Caballol, N.; Martí, M. J.; Tolosa, E. Cognitive Dysfunction and Dementia in Parkinson Disease. *Mov. Disord.* **2007**, *22* (S17), S358–S366. https://doi.org/10.1002/mds.21677.

(36) Josviak, N. D.; Batistela, M. S.; Souza, R. K. M.; Wegner, N. R.; Bono, G. F.;

Sulzbach, C. D.; Simão-Silva, D. P.; Piovezan, M. R.; Souza, R. L. R.; Furtado-Alle, L. Plasma Butyrylcholinesterase Activity: A Possible Biomarker for Differential Diagnosis between Alzheimer's Disease and Dementia with Lewy Bodies? *Int. J. Neurosci.* **2017**, *127* (12), 1082–1086. https://doi.org/10.1080/00207454.2017.1329203.

(37) Sun, Y.; Wang, P.; Zheng, H.; Smith, R. G. Ghrelin Stimulation of Growth Hormone Release and Appetite Is Mediated through the Growth Hormone Secretagogue Receptor. *Proc. Natl. Acad. Sci.* **2004**, *101* (13), 4679–4684. https://doi.org/10.1073/pnas.0305930101.

(38) De Vriese, C.; Gregoire, F.; Lema-Kisoka, R.; Waelbroeck, M.; Robberecht, P.; Delporte, C. Ghrelin Degradation by Serum and Tissue Homogenates: Identification of the Cleavage Sites. *Endocrinology* **2004**, *145* (11), 4997–5005. https://doi.org/10.1210/en.2004-0569.

(39) Dorling, J. L.; Clayton, D. J.; Jones, J.; Carter, W. G.; Thackray, A. E.; King, J. A.; Pucci, A.; Batterham, R. L.; Stensel, D. J. A Randomized Crossover Trial Assessing the Effects of Acute Exercise on Appetite, Circulating Ghrelin Concentrations, and Butyrylcholinesterase Activity in Normal-Weight Males with Variants of the Obesity-Linked FTO Rs9939609 Polymorphism. *Am. J. Clin. Nutr.* **2019**, *110* (5), 1055–1066. https://doi.org/10.1093/ajcn/nqz188.

(40) Chen, V. P.; Gao, Y.; Geng, L.; Brimijoin, S. Butyrylcholinesterase Regulates Central Ghrelin Signaling and Has an Impact on Food Intake and Glucose Homeostasis. *Int. J. Obes.* **2017**, *41* (9), 1413–1419. https://doi.org/10.1038/ijo.2017.123.

(41) Chen, V. P.; Gao, Y.; Geng, L.; Parks, R. J.; Pang, Y.-P.; Brimijoin, S. Plasma Butyrylcholinesterase Regulates Ghrelin to Control Aggression. *Proc. Natl. Acad. Sci.* **2015**, *112* (7), 2251–2256. https://doi.org/10.1073/pnas.1421536112.

(42) Spencer, S. J.; Xu, L.; Clarke, M. A.; Lemus, M.; Reichenbach, A.; Geenen, B.; Kozicz, T.; Andrews, Z. B. Ghrelin Regulates the Hypothalamic-Pituitary-Adrenal Axis and Restricts Anxiety After Acute Stress. *Biol. Psychiatry* **2012**, *72* (6), 457–465. https://doi.org/10.1016/j.biopsych.2012.03.010.

(43) Jbilo, O.; Bartels, C. F.; Chatonnet, A.; Toutant, J. P.; Lockridge, O. Tissue Distribution of Human Acetylcholinesterase and Butyrylcholinesterase Messenger RNA. *Toxicon* **1994**, *32* (11), 1445–1457.

https://doi.org/10.1016/0041-0101(94)90416-2.

(44) Pohanka, M. Butyrylcholinesterase as a Biochemical Marker. *Bratisl. Lek. Listy* **2013**, *114* (12), 726–734. https://doi.org/10.4149/bll_2013_153.

(45) Lockridge, O.; Masson, P. Pesticides and Susceptible Populations: People with Butyrylcholinesterase Genetic Variants May Be at Risk. *Neurotoxicology* **2000**, *21* (1–2), 113–126. https://doi.org/10794391.

(46) Saxena, A.; Sun, W.; Luo, C.; Myers, T. M.; Koplovitz, I.; Lenz, D. E.; Doctor, B. P. Bioscavenger for Protection From Toxicity of Organophosphorus Compounds. *J. Mol. Neurosci.* **2006**, *30* (1–2), 145–148. https://doi.org/10.1385/JMN:30:1:145.

(47) Duysen, E. G.; Li, B.; Darvesh, S.; Lockridge, O. Sensitivity of Butyrylcholinesterase Knockout Mice to (−)-Huperzine A and Donepezil Suggests Humans with Butyrylcholinesterase Deficiency May Not Tolerate These Alzheimer's Disease Drugs and Indicates Butyrylcholinesterase Function in Neurotransmission. *Toxicology* **2007**, *233* (1–3), 60–69. https://doi.org/10.1016/j.tox.2006.11.069.

(48) Lockridge, O.; Duysen, E. G.; Voelker, T.; Thompson, C. M.; Schopfer, L. M. Life without Acetylcholinesterase: The Implications of Cholinesterase Inhibitor Toxicity in AChE-Knockout Mice. *Environ. Toxicol. Pharmacol.* **2005**, *19* (3), 463–469. https://doi.org/10.1016/j.etap.2004.12.008.

(49) Kamendulis, L. M.; Brzezinski, M. R.; Pindel, E. V; Bosron, W. F.; Dean, R. A. Metabolism of Cocaine and Heroin Is Catalyzed by the Same Human Liver Carboxylesterases. *J. Pharmacol. Exp. Ther.* **1996**, *279* (2), 713–717.

(50) Cohen-Barak, O.; Wildeman, J.; van de Wetering, J.; Hettinga, J.; Schuilenga-Hut, P.; Gross, A.; Clark, S.; Bassan, M.; Gilgun-Sherki, Y.; Mendzelevski, B.; Spiegelstein, O. Safety, Pharmacokinetics, and Pharmacodynamics of TV-1380, a Novel Mutated Butyrylcholinesterase Treatment for Cocaine Addiction, after Single and Multiple Intramuscular Injections in Healthy Subjects. *J. Clin. Pharmacol.* **2015**, *55* (5), 573–583. https://doi.org/10.1002/jcph.450.

(51) Mattes, C. E.; Lynch, T. J.; Singh, A.; Bradley, R. M.; Kellaris, P. A.; Brady, R. O.; Dretchen, K. L. Therapeutic Use of Butyrylcholinesterase for Cocaine Intoxication. *Toxicol. Appl. Pharmacol.* **1997**, *145* (2), 372–380. https://doi.org/10.1006/taap.1997.8188.

(52) McGehee, D. S.; Krasowski, M. D.; Fung, D. L.; Wilson, B.; Gronert, G. A.; Moss, J. Cholinesterase Inhibition by Potato Glycoalkaloids Slows Mivacurium Metabolism. *Anesthesiology* **2000**, *93* (2), 510–519. https://doi.org/10.1097/00000542-200008000-00031.

(53) Howes, M.-J. R.; Perry, N. S. L.; Houghton, P. J. Plants with Traditional Uses and Activities, Relevant to the Management of Alzheimer's Disease and Other Cognitive Disorders. *Phytother. Res.* **2003**, *17* (1), 1–18. https://doi.org/10.1002/ptr.1280.

(54) I. Erdogan Orhan. Current Concepts on Selected Plant Secondary Metabolites With Promising Inhibitory Effects Against Enzymes Linked to Alzheimer's Disease. *Curr. Med. Chem.* **2012**, *19* (14), 2252–2261. https://doi.org/10.2174/092986712800229032.

(55) Zhang, B.; Yu, H.; Lu, W.; Yu, B.; Liu, L.; Jia, W.; Lin, Z.; Wang, H.; Chen, S. Four New Honokiol Derivatives from the Stem Bark of Magnolia Officinalis and Their Anticholinesterase Activities. *Phytochem. Lett.* **2019**, *29*, 195–198. https://doi.org/10.1016/j.phytol.2018.12.015.

(56) Singh, S.; Kumar, V.; Thakur, S.; Banerjee, B. D.; Chandna, S.; Rautela, R. S.; Grover, S. S.; Rawat, D. S.; Pasha, S. T.; Jain, S. K.; Ichhpujani, R. L.; Rai, A. DNA Damage and Cholinesterase Activity in Occupational Workers Exposed to Pesticides. *Environ. Toxicol. Pharmacol.* **2011**, *31* (2), 278–285. https://doi.org/10.1016/j.etap.2010.11.005.

(57) Alavanja, M. C. R.; Bonner, M. R. Occupational Pesticide Exposures and Cancer Risk: A Review. *J. Toxicol. Environ. Heal. Part B* **2012**, *15* (4), 238–263. https://doi.org/10.1080/10937404.2012.632358.

(58) Matich, E. K.; Laryea, J. A.; Seely, K. A.; Stahr, S.; Su, L. J.; Hsu, P.-C. Association between Pesticide Exposure and Colorectal Cancer Risk and Incidence: A Systematic Review. *Ecotoxicol. Environ. Saf.* **2021**, *219*, 112327. https://doi.org/10.1016/j.ecoenv.2021.112327.

(59) Rowland, A. S. Pesticides and Birth Defects. *Epidemiology* **1995**, *6* (1), 6–7.

(60) Roberts, J. R.; Karr, C. J.; Council On Environmental Health. Pesticide Exposure in Children. *Pediatrics* **2012**, *130* (6), e1765-88. https://doi.org/10.1542/peds.2012-2758.

(61) Xu, Q.; Zhu, B.; Dong, X.; Li, S.; Song, X.; Xiao, X.; Zhang, C.; Lv, Y.; Zhang,

X.; Li, Y. Pyrethroid Pesticide Exposure during Early Pregnancy and Birth Outcomes in Southwest China: A Birth Cohort Study. *J. Toxicol. Sci.* **2020**, *45* (5), 281–291. https://doi.org/10.2131/jts.45.281.

(62) Ziegler, D. M. The 1990 Bernard B. Brodie Award Lecture. Unique Properties of the Enzymes of Detoxication. *Drug Metab. Dispos.* **1991**, *19* (5), 847–852.

(63) Darvesh, S.; Darvesh, K. V.; McDonald, R. S.; Mataija, D.; Walsh, R.; Mothana, S.; Lockridge, O.; Martin, E. Carbamates with Differential Mechanism of Inhibition Toward Acetylcholinesterase and Butyrylcholinesterase. *J. Med. Chem.* **2008**, *51* (14), 4200–4212. https://doi.org/10.1021/jm8002075.

(64) Bodur, E.; Cokugras, A. N. (16) The Effects of Indole-3-Acetic Acid on Human and Horse Serum Butyrylcholinesterase. *Chem. Biol. Interact.* **2005**, *157–158*, 375–378. https://doi.org/10.1016/j.cbi.2005.10.061.

(65) Raveh, L.; Grauer, E.; Grunwald, J.; Cohen, E.; Ashani, Y. The Stoichiometry of Protection against Soman and VX Toxicity in Monkeys Pretreated with Human Butyrylcholinesterase. *Toxicol. Appl. Pharmacol.* **1997**, *145* (1), 43–53. https://doi.org/10.1006/taap.1997.8160.

(66) Ogunkeye, O. O.; Roluga, A. I. Serum Cholinesterase Activity Helps to Distinguish between Liver Disease and Non-Liver Disease Aberration in Liver Function Tests. *Pathophysiology* **2006**, *13* (2), 91–93. https://doi.org/10.1016/j.pathophys.2006.01.002.

(67) Gu, S.-Z. Alterations of Serum Cholinesterase in Patients with Gastric Cancer. *World J. Gastroenterol.* **2005**, *11* (29), 4604. https://doi.org/10.3748/wjg.v11.i29.4604.

(68) Poetsch, N.; Sturdza, A.; Aust, S.; Polterauer, S.; Grimm, C.; Schwameis, R.; Pötter, R.; Koelbl, H.; Reinthaller, A.; Seebacher, V. The Value of Pretreatment Serum Butyrylcholinesterase Level as a Novel Prognostic Biomarker in Patients with Cervical Cancer Treated with Primary (Chemo-)Radiation Therapy. *Strahlenther. Onkol.* **2019**, *195* (5), 430–440. https://doi.org/10.1007/s00066-019-01430-z.

(69) Gu, Y.; Chow, M. J.; Kapoor, A.; Mei, W.; Jiang, Y.; Yan, J.; De Melo, J.; Seliman, M.; Yang, H.; Cutz, J.-C.; Bonert, M.; Major, P.; Tang, D. Biphasic Alteration of Butyrylcholinesterase (BChE) During Prostate Cancer Development. *Transl. Oncol.* **2018**, *11* (4), 1012–1022.

https://doi.org/10.1016/j.tranon.2018.06.003.

(70) Cadenas, E. BIOLOGICAL CHEMILUMINESCENCE. *Photochem. Photobiol.* **1984**, *40* (6), 823–830. https://doi.org/10.1111/j.1751-1097.1984.tb04657.x.

(71) Syed, A. J.; Anderson, J. C. Applications of Bioluminescence in Biotechnology and Beyond. *Chem. Soc. Rev.* **2021**, *50* (9), 5668–5705. https://doi.org/10.1039/d0cs01492c.

(72) Vacher, M.; Fdez. Galván, I.; Ding, B.-W.; Schramm, S.; Berraud-Pache, R.; Naumov, P.; Ferré, N.; Liu, Y.-J.; Navizet, I.; Roca-Sanjuán, D.; Baader, W. J.; Lindh, R. Chemi- and Bioluminescence of Cyclic Peroxides. *Chem. Rev.* **2018**, *118* (15), 6927–6974. https://doi.org/10.1021/acs.chemrev.7b00649.

(73) Delafresnaye, L.; Bloesser, F. R.; Kockler, K. B.; Schmitt, C. W.; Irshadeen, I. M.; Barner-Kowollik, C. All Eyes on Visible-Light Peroxyoxalate Chemiluminescence Read-Out Systems. *Chem. – A Eur. J.* **2020**, *26* (1), 114–127. https://doi.org/10.1002/chem.201904054.

(74) Li, B.; Kim, Y. L.; Lippert, A. R. Chemiluminescence Measurement of Reactive Sulfur and Nitrogen Species. *Antioxid. Redox Signal.* **2022**, *36* (4–6), 337–353. https://doi.org/10.1089/ars.2021.0195.

(75) Albrecht, H. O. Über Die Chemiluminescenz Des Aminophthalsäurehydrazids. *Zeitschrift für Phys. Chemie* **1928**, *136U* (1), 321–330. https://doi.org/10.1515/zpch-1928-13625.

(76) Khan, P.; Idrees, D.; Moxley, M. A.; Corbett, J. A.; Ahmad, F.; von Figura, G.; Sly, W. S.; Waheed, A.; Hassan, M. I. Luminol-Based Chemiluminescent Signals: Clinical and Non-Clinical Application and Future Uses. *Appl. Biochem. Biotechnol.* **2014**, *173* (2), 333–355. https://doi.org/10.1007/s12010-014-0850-1.

(77) Malin Emteborg (b. Stigbrand); Pontén, E.; Irgum, K. Influence of Imidazole and Bis(Trichlorophenyl) Oxalate in the Oxalyldiimidazole Peroxyoxalate Chemiluminescence Reaction. *Anal. Chem.* **1997**, *69* (11), 2109–2114. https://doi.org/10.1021/ac961225o.

(78) Park, S.; Kwon, O.-H.; Kim, S.; Park, S.; Choi, M.-G.; Cha, M.; Park, S. Y.; Jang, D.-J. Imidazole-Based Excited-State Intramolecular Proton-Transfer Materials: Synthesis and Amplified Spontaneous Emission from a Large Single Crystal. *J. Am. Chem. Soc.* **2005**, *127* (28), 10070–10074. https://doi.org/10.1021/ja0508727.

(79) Kellogg, R. E. Mechanism of Chemiluminescence from Peroxy Radicals. *J. Am. Chem. Soc.* **1969**, *91* (20), 5433–5436. https://doi.org/10.1021/ja01048a005.

(80) Haris, U.; Lippert, A. R. Exploring the Structural Space of Chemiluminescent 1,2-Dioxetanes. *ACS Sensors* **2023**, *8* (1), 3–11. https://doi.org/10.1021/acssensors.2c02371.

(81) Green, O.; Eilon, T.; Hananya, N.; Gutkin, S.; Bauer, C. R.; Shabat, D. Opening a Gateway for Chemiluminescence Cell Imaging: Distinctive Methodology for Design of Bright Chemiluminescent Dioxetane Probes. *ACS Cent. Sci.* **2017**, *3* (4), 349–358. https://doi.org/10.1021/acscentsci.7b00058.

(82) Schaap, A. P.; Chen, T.-S.; Handley, R. S.; DeSilva, R.; Giri, B. P. Chemical and Enzymatic Triggering of 1,2-Dioxetanes. 2: Fluoride-Induced Chemiluminescence from Tert-Butyldimethylsilyloxy-Substituted Dioxetanes. *Tetrahedron Lett.* **1987**, *28* (11), 1155–1158. https://doi.org/10.1016/S0040-4039(00)95313-9.

(83) Schaap, A. P.; Handley, R. S.; Giri, B. P. Chemical and Enzymatic Triggering of 1,2-Dioxetanes. 1: Aryl Esterase-Catalyzed Chemiluminescence from a Naphthyl Acetate-Substituted Dioxetane. *Tetrahedron Lett.* **1987**, *28* (9), 935–938. https://doi.org/10.1016/S0040-4039(00)95878-7.

(84) Schaap, A. P.; Sandison, M. D.; Handley, R. S. Chemical and Enzymatic Triggering of 1,2-Dioxetanes. 3: Alkaline Phosphatase-Catalyzed Chemiluminescence from an Aryl Phosphate-Substituted Dioxetane. *Tetrahedron Lett.* **1987**, *28* (11), 1159–1162. https://doi.org/10.1016/S0040-4039(00)95314-0.

(85) Bronstein, I.; Edwards, B.; Voyta, J. C. 1,2-Dioxetanes: Novel Chemiluminescent Enzyme Substrates. Applications to Immunoassays. *J. Biolumin. Chemilumin.* **1989**, *4* (1), 99–111. https://doi.org/10.1002/bio.1170040116.

(86) Gnaim, S.; Green, O.; Shabat, D. The Emergence of Aqueous Chemiluminescence: New Promising Class of Phenoxy 1,2-Dioxetane Luminophores. *Chem. Commun.* **2018**, *54* (17), 2073–2085. https://doi.org/10.1039/C8CC00428E.

(87) Cao, J.; Lopez, R.; Thacker, J. M.; Moon, J. Y.; Jiang, C.; Morris, S. N. S.; Bauer, J. H.; Tao, P.; Mason, R. P.; Lippert, A. R. Chemiluminescent Probes for Imaging H 2 S in Living Animals. *Chem. Sci.* **2015**, *6* (3), 1979–1985. https://doi.org/10.1039/C4SC03516J.

(88) Hananya, N.; Green, O.; Blau, R.; Satchi-Fainaro, R.; Shabat, D. A Highly Efficient Chemiluminescence Probe for the Detection of Singlet Oxygen in Living Cells. *Angew. Chemie Int. Ed.* **2017**, *56* (39), 11793–11796. https://doi.org/10.1002/anie.201705803.

(89) Shelef, O.; Sedgwick, A. C.; Pozzi, S.; Green, O.; Satchi-Fainaro, R.; Shabat, D.; Sessler, J. L. Turn on Chemiluminescence-Based Probes for Monitoring Tyrosinase Activity in Conjunction with Biological Thiols. *Chem. Commun.* **2021**, *57* (86), 11386–11389. https://doi.org/10.1039/D1CC05217A.

(90) Ozsan, C.; Kailass, K.; Digby, E. M.; Almammadov, T.; Beharry, A. A.; Kolemen, S. Selective Detection of Carboxylesterase 2 Activity in Cancer Cells Using an Activity-Based Chemiluminescent Probe. *Chem. Commun.* **2022**, *58* (78), 10929–10932. https://doi.org/10.1039/D2CC03309G.

(91) Cao, J.; Campbell, J.; Liu, L.; Mason, R. P.; Lippert, A. R. In Vivo Chemiluminescent Imaging Agents for Nitroreductase and Tissue Oxygenation. *Anal. Chem.* **2016**, *88* (9), 4995–5002. https://doi.org/10.1021/acs.analchem.6b01096.

(92) Ryan, L. S.; Gerberich, J.; Cao, J.; An, W.; Jenkins, B. A.; Mason, R. P.; Lippert, A. R. Kinetics-Based Measurement of Hypoxia in Living Cells and Animals Using an Acetoxymethyl Ester Chemiluminescent Probe. *ACS Sensors* **2019**, *4* (5), 1391–1398. https://doi.org/10.1021/acssensors.9b00360.

(93) Sun, J.; Hu, Z.; Wang, R.; Zhang, S.; Zhang, X. A Highly Sensitive Chemiluminescent Probe for Detecting Nitroreductase and Imaging in Living Animals. *Anal. Chem.* **2019**, *91* (2), 1384–1390. https://doi.org/10.1021/acs.analchem.8b03955.

(94) Wang, B.; Chen, Z.; Cen, X.; Liang, Y.; Tan, L.; Liang, E.; Zheng, L.; Zheng, Y.; Zhan, Z.; Cheng, K. A Highly Selective and Sensitive Chemiluminescent Probe for Leucine Aminopeptidase Detection in Vitro , in Vivo and in Human Liver Cancer Tissue. *Chem. Sci.* **2022**, *13* (8), 2324–2330. https://doi.org/10.1039/D1SC06528A.

(95) Gunduz, H.; Acari, A.; Cetin, S.; Almammadov, T.; Pinarbasi-Degirmenci, N.; Dirak, M.; Cingoz, A.; Kilic, E.; Bagci-Onder, T.; Kolemen, S. Directing Chemiluminescent Dioxetanes to Mitochondria: A Cationic Luminophore Enables in Vitro and in Vivo Detection of Cancer Cells upon Enzymatic

Activation. *Sensors Actuators B Chem.* **2023**, *383*, 133574. https://doi.org/10.1016/j.snb.2023.133574.

(96) Ye, S.; Hananya, N.; Green, O.; Chen, H.; Zhao, A. Q.; Shen, J.; Shabat, D.; Yang, D. A Highly Selective and Sensitive Chemiluminescent Probe for Real-Time Monitoring of Hydrogen Peroxide in Cells and Animals. *Angew. Chemie Int. Ed.* **2020**, *59* (34), 14326–14330. https://doi.org/10.1002/anie.202005429.

(97) Ye, S.; Yang, B.; Wu, M.; Chen, Z.; Shen, J.; Shabat, D.; Yang, D. Recurring Real-Time Monitoring of Inflammations in Living Mice with a Chemiluminescent Probe for Hypochlorous Acid. *CCS Chem.* **2022**, *4* (6), 1871–1878. https://doi.org/10.31635/ccschem.021.202101108.

(98) An, W.; Ryan, L. S.; Reeves, A. G.; Bruemmer, K. J.; Mouhaffel, L.; Gerberich, J. L.; Winters, A.; Mason, R. P.; Lippert, A. R. A Chemiluminescent Probe for HNO Quantification and Real-Time Monitoring in Living Cells. *Angew. Chemie Int. Ed.* **2019**, *58* (5), 1361–1365. https://doi.org/10.1002/anie.201811257.

(99) Kagalwala, H. N.; Gerberich, J.; Smith, C. J.; Mason, R. P.; Lippert, A. R. Chemiluminescent 1,2-Dioxetane Iridium Complexes for Near-Infrared Oxygen Sensing. *Angew. Chemie Int. Ed.* **2022**, *61* (12). https://doi.org/10.1002/anie.202115704.

(100) Kagalwala, H. N.; Bueno, L.; Wanniarachchi, H.; Unruh, D. K.; Hamal, K. B.; Pavlich, C. I.; Carlson, G. J.; Pinney, K. G.; Mason, R. P.; Lippert, A. R. Oxygen-Sensing Chemiluminescent Iridium(III) 1,2-Dioxetanes: Unusual Coordination and Activity. *Anal. Sens.* **2023**, *3* (1). https://doi.org/10.1002/anse.202200085.

(101) Cheng, P.; Miao, Q.; Li, J.; Huang, J.; Xie, C.; Pu, K. Unimolecular Chemo-Fluoro-Luminescent Reporter for Crosstalk-Free Duplex Imaging of Hepatotoxicity. *J. Am. Chem. Soc.* **2019**, *141* (27), 10581–10584. https://doi.org/10.1021/jacs.9b02580.

(102) Cao, J.; An, W.; Reeves, A. G.; Lippert, A. R. A Chemiluminescent Probe for Cellular Peroxynitrite Using a Self-Immolative Oxidative Decarbonylation Reaction. *Chem. Sci.* **2018**, *9* (9), 2552–2558. https://doi.org/10.1039/C7SC05087A.

(103) Huang, J.; Huang, J.; Cheng, P.; Jiang, Y.; Pu, K. Near-Infrared Chemiluminescent Reporters for In Vivo Imaging of Reactive Oxygen and

Nitrogen Species in Kidneys. *Adv. Funct. Mater.* **2020**, *30* (39), 2003628. https://doi.org/10.1002/adfm.202003628.

(104) Levinn, C. M.; Pluth, M. D. Direct Comparison of Triggering Motifs on Chemiluminescent Probes for Hydrogen Sulfide Detection in Water. *Sensors Actuators B Chem.* **2021**, *329*, 129235. https://doi.org/10.1016/j.snb.2020.129235.

(105) Sun, J.; Hu, Z.; Zhang, S.; Zhang, X. A Novel Chemiluminescent Probe Based on 1,2-Dioxetane Scaffold for Imaging Cysteine in Living Mice. *ACS Sensors* **2019**, *4* (1), 87–92. https://doi.org/10.1021/acssensors.8b00936.

(106) Fu, A.; Mao, Y.; Wang, H.; Cao, Z. An Activatable Chemiluminescence Probe Based on Phenoxy-Dioxetane Scaffold for Biothiol Imaging in Living Systems. *J. Pharm. Biomed. Anal.* **2021**, *204*, 114266. https://doi.org/10.1016/j.jpba.2021.114266.

(107) Ryan, L. S.; Gerberich, J.; Haris, U.; Nguyen, D.; Mason, R. P.; Lippert, A. R. Ratiometric PH Imaging Using a 1,2-Dioxetane Chemiluminescence Resonance Energy Transfer Sensor in Live Animals. *ACS Sensors* **2020**, *5* (9), 2925–2932. https://doi.org/10.1021/acssensors.0c01393.

(108) Hananya, N.; Eldar Boock, A.; Bauer, C. R.; Satchi-Fainaro, R.; Shabat, D. Remarkable Enhancement of Chemiluminescent Signal by Dioxetane–Fluorophore Conjugates: Turn-ON Chemiluminescence Probes with Color Modulation for Sensing and Imaging. *J. Am. Chem. Soc.* **2016**, *138* (40), 13438–13446. https://doi.org/10.1021/jacs.6b09173.

(109) Green, O.; Gnaim, S.; Blau, R.; Eldar-Boock, A.; Satchi-Fainaro, R.; Shabat, D. Near-Infrared Dioxetane Luminophores with Direct Chemiluminescence Emission Mode. *J. Am. Chem. Soc.* **2017**, *139* (37), 13243–13248. https://doi.org/10.1021/jacs.7b08446.

(110) Cui, D.; Li, J.; Zhao, X.; Pu, K.; Zhang, R. Semiconducting Polymer Nanoreporters for Near-Infrared Chemiluminescence Imaging of Immunoactivation. *Adv. Mater.* **2020**, *32* (6), 1906314. https://doi.org/10.1002/adma.201906314.

(111) Gnaim, S.; Scomparin, A.; Eldar-Boock, A.; Bauer, C. R.; Satchi-Fainaro, R.; Shabat, D. Light Emission Enhancement by Supramolecular Complexation of Chemiluminescence Probes Designed for Bioimaging. *Chem. Sci.* **2019**, *10* (10),

2945–2955. https://doi.org/10.1039/C8SC05174G.

(112) Kagalwala, H. N.; Lippert, A. R. Energy Transfer Chemiluminescent Spiroadamantane 1,2-Dioxetane Probes for Bioanalyte Detection and Imaging. *Angew. Chemie Int. Ed.* **2022**, *61* (42). https://doi.org/10.1002/anie.202210057.

(113) Ellman, G. L.; Courtney, K. D.; Andres, V.; Featherstone, R. M. A New and Rapid Colorimetric Determination of Acetylcholinesterase Activity. *Biochem. Pharmacol.* **1961**, *7* (2), 88–95. https://doi.org/10.1016/0006-2952(61)90145-9.

(114) Komersová, A.; Komers, K.; Čegan, A. New Findings about Ellman's Method to Determine Cholinesterase Activity. *Zeitschrift für Naturforsch. C* **2007**, *62* (1–2), 150–154. https://doi.org/10.1515/znc-2007-1-225.

(115) Šinko, G.; Čalić, M.; Bosak, A.; Kovarik, Z. Limitation of the Ellman Method: Cholinesterase Activity Measurement in the Presence of Oximes. *Anal. Biochem.* **2007**, *370* (2), 223–227. https://doi.org/10.1016/j.ab.2007.07.023.

(116) Pohanka, M.; Hrabinova, M.; Kuca, K.; Simonato, J.-P. Assessment of Acetylcholinesterase Activity Using Indoxylacetate and Comparison with the Standard Ellman's Method. *Int. J. Mol. Sci.* **2011**, *12* (4), 2631–2640. https://doi.org/10.3390/ijms12042631.

(117) Dingova, D.; Leroy, J.; Check, A.; Garaj, V.; Krejci, E.; Hrabovska, A. Optimal Detection of Cholinesterase Activity in Biological Samples: Modifications to the Standard Ellman's Assay. *Anal. Biochem.* **2014**, *462*, 67–75. https://doi.org/10.1016/j.ab.2014.05.031.

(118) Miao, Y.; He, N.; Zhu, J.-J. History and New Developments of Assays for Cholinesterase Activity and Inhibition. *Chem. Rev.* **2010**, *110* (9), 5216–5234. https://doi.org/10.1021/cr900214c.

(119) Holas, O.; Musilek, K.; Pohanka, M.; Kuca, K. The Progress in the Cholinesterase Quantification Methods. *Expert Opin. Drug Discov.* **2012**, *7* (12), 1207–1223. https://doi.org/10.1517/17460441.2012.729037.

(120) Augustinsson, K.-B. Assay Methods for Cholinesterases; 2006; pp 1–63. https://doi.org/10.1002/9780470110218.ch1.

(121) Bach, P. H.; Wingfield, E. Sandra; Leary, W. P.; Bach, F.; Turner, H. Assessment of a Diagnostic Dip-Stick for Assaying Plasma or Serum Pseudocholinesterase Activity. *South African Med. J.* **1978**, *54* (3), 108–112.

(122) Fischl, J.; Pinto, N.; Gordon, C. Rapid Detection of Organic Phosphorus Poisons.

Clin. Chem. **1968**, *14* (4), 371–373.

(123) White, B. J.; Andrew Legako, J.; James Harmon, H. Spectrophotometric Detection of Cholinesterase Inhibitors with an Integrated Acetyl-/Butyrylcholinesterase Surface. *Sensors Actuators B Chem.* **2003**, *89* (1–2), 107–111. https://doi.org/10.1016/S0925-4005(02)00450-1.

(124) Makower, A.; Halámek, J.; Skládal, P.; Kernchen, F.; Scheller, F. W. New Principle of Direct Real-Time Monitoring of the Interaction of Cholinesterase and Its Inhibitors by Piezolectric Biosensor. *Biosens. Bioelectron.* **2003**, *18* (11), 1329–1337. https://doi.org/10.1016/S0956-5663(03)00089-7.

(125) Johnson, C. D.; Russell, R. L. A Rapid, Simple Radiometric Assay for Cholinesterase, Suitable for Multiple Determinations. *Anal. Biochem.* **1975**, *64* (1), 229–238. https://doi.org/10.1016/0003-2697(75)90423-6.

(126) Pohanka, M. Voltammetric Assay of Butyrylcholinesterase in Plasma Samples and Its Comparison to the Standard Spectrophotometric Test. *Talanta* **2014**, *119*, 412–416. https://doi.org/10.1016/j.talanta.2013.11.045.

(127) Brock, A.; Mortensen, V.; Rasmussen Loft, A. G.; Nørgaard-Pedersen, B. Enzyme Immunoassay of Human Cholinesterase (EC 3.1.1.8) Comparison of Immunoreactive Substance Concentration with Catalytic Activity Concentration in Randomly Selected Serum Samples from Healthy Individuals. *Clin. Chem. Lab. Med.* **1990**, *28* (4). https://doi.org/10.1515/cclm.1990.28.4.221.

(128) Khattab, A. D.; Walker, C. H.; Johnston, G.; Siddiqui, M. K.; Saphier, P. W. An Elisa Assay for Avian Serum Butyrylcholinesterase: A Biomarker for Organophosphates. *Environ. Toxicol. Chem.* **1994**, *13* (10), 1661–1667. https://doi.org/10.1002/etc.5620131016.

(129) Yang, S.-H.; Sun, Q.; Xiong, H.; Liu, S.-Y.; Moosavi, B.; Yang, W.-C.; Yang, G.-F. Discovery of a Butyrylcholinesterase-Specific Probe via a Structure-Based Design Strategy. *Chem. Commun.* **2017**, *53* (28), 3952–3955. https://doi.org/10.1039/C7CC00577F.

(130) Liu, S.-Y.; Xiong, H.; Yang, J.-Q.; Yang, S.-H.; Li, Y.; Yang, W.-C.; Yang, G.-F. Discovery of Butyrylcholinesterase-Activated Near-Infrared Fluorogenic Probe for Live-Cell and In Vivo Imaging. *ACS Sensors* **2018**, *3* (10), 2118–2128. https://doi.org/10.1021/acssensors.8b00697.

(131) Chen, G.; Feng, H.; Xi, W.; Xu, J.; Pan, S.; Qian, Z. Thiol–ene Click Reaction-

Induced Fluorescence Enhancement by Altering the Radiative Rate for Assaying Butyrylcholinesterase Activity. *Analyst* **2019**, *144* (2), 559–566. https://doi.org/10.1039/C8AN01808A.

(132) Yoo, S.; Han, M. S. A Fluorescent Probe for Butyrylcholinesterase Activity in Human Serum Based on a Fluorophore with Specific Binding Affinity for Human Serum Albumin. *Chem. Commun.* **2019**, *55* (97), 14574–14577. https://doi.org/10.1039/C9CC07737E.

(133) Ma, Y.; Gao, W.; Ma, S.; Liu, Y.; Lin, W. Observation of the Elevation of Cholinesterase Activity in Brain Glioma by a Near-Infrared Emission Chemsensor. *Anal. Chem.* **2020**, *92* (19), 13405–13410. https://doi.org/10.1021/acs.analchem.0c02770.

(134) Cao, T.; Zheng, L.; Zhang, L.; Teng, Z.; Qian, J.; Ma, H.; Wang, J.; Cao, Y.; Qin, W.; Liu, Y. A Highly Butyrylcholinesterase Selective Red-Emissive Mitochondria-Targeted Fluorescent Indicator Imaging in Liver Tissue of Mice. *Sensors Actuators B Chem.* **2021**, *330*, 129348. https://doi.org/10.1016/j.snb.2020.129348.

(135) Zhang, Q.; Fu, C.; Guo, X.; Gao, J.; Zhang, P.; Ding, C. Fluorescent Determination of Butyrylcholinesterase Activity and Its Application in Biological Imaging and Pesticide Residue Detection. *ACS Sensors* **2021**, *6* (3), 1138–1146. https://doi.org/10.1021/acssensors.0c02398.

(136) Wan, C.; Li, J.; Gao, J.; Liu, H.; Zhang, Q.; Zhang, P.; Ding, C. Ratiometric Fluorescence Assay for Butyrylcholinesterase Activity Based on a Hemicyanine and Its Application in Biological Imaging. *Dye. Pigment.* **2022**, *197*, 109874. https://doi.org/10.1016/j.dyepig.2021.109874.

(137) Xiang, C.; Xiang, J.; Yang, X.; Li, C.; Zhou, L.; Jiang, D.; Peng, Y.; Xu, Z.; Deng, G.; Zhu, B.; Zhang, P.; Cai, L.; Gong, P. Ratiometric Imaging of Butyrylcholinesterase Activity in Mice with Nonalcoholic Fatty Liver Using an AIE-Based Fluorescent Probe. *J. Mater. Chem. B* **2022**, *10* (22), 4254–4260. https://doi.org/10.1039/D2TB00422D.

(138) Zhang, W.; Zhang, J.; Qin, C.; Wang, X.; Zhou, Y. A Far-Red/near-Infrared Fluorescence Probe with Large Stokes Shift for Monitoring Butyrylcholinesterase (BChE) in Living Cells and in Vivo. *Anal. Chim. Acta* **2022**, *1235*, 340540. https://doi.org/10.1016/j.aca.2022.340540.

(139) Zhang, P.; Fu, C.; Liu, H.; Guo, X.; Zhang, Q.; Gao, J.; Chen, W.; Yuan, W.; Ding, C. AND-Logic Strategy for Accurate Analysis of Alzheimer's Disease via Fluorescent Probe Lighted Up by Two Specific Biomarkers. *Anal. Chem.* **2021**, *93* (32), 11337–11345. https://doi.org/10.1021/acs.analchem.1c02943.

(140) Yang, Y.; Zhang, L.; Wang, J.; Cao, Y.; Li, S.; Qin, W.; Liu, Y. Diagnosis of Alzheimer's Disease and In Situ Biological Imaging via an Activatable Near-Infrared Fluorescence Probe. *Anal. Chem.* **2022**, *94* (39), 13498–13506. https://doi.org/10.1021/acs.analchem.2c02627.

(141) Pei, X.; Fang, Y.; Gu, H.; Zheng, S.; Bin, X.; Wang, F.; He, M.; Lu, S.; Chen, X. A Turn-on Fluorescent Probe Based on ESIPT and AIEE Mechanisms for the Detection of Butyrylcholinesterase Activity in Living Cells and in Non-Alcoholic Fatty Liver of Zebrafish. *Spectrochim. Acta Part A Mol. Biomol. Spectrosc.* **2023**, *287*, 122044. https://doi.org/10.1016/j.saa.2022.122044.

Appendix A: Literature Comparison of Recently Published Fluorescence Probes for the Detection of BChE

Name	Detection Limit	Type	*In vivo* Applicability	References
BChE-FP	N/A	Fluorophore	N/A	Chem.Commun. **2017**, 53, 3952
BChE-NIRFP	N/A	Fluorophore	Zebra Fish Model Alzheimer's disease model via prefrontal cortex injection	ACS. Sens. **2018**, 3, 2118
DCPDA	60 U/L	Fluorophore	N/A	Analyst. **2019**, 144, 559
DSC	1.2 U/L	Fluorophore	N/A	Chem.Commun. **2019**, 55, 14574
IPAN	11.7 U/L	Fluorophore	Zebra Fish Model	Anal. Chem. **2020**, 92, 13405
CyCICP	3.75 U/L	Fluorophore	N/A	Talanta. **2020**, 219, 121278
BChE-NBD	29 ng/mL	Fluorophore	Mouse Liver Imaging	Sensors and Actuators B: Chemical. **2021**, 330, 129348
P1	0.8 U/mL	Fluorophore	Healthy Mouse Brain Imaging via prefrontal cortex injection	ACS. Sens. **2021**, 6, 1138
P1	1.08 μg/mL	Fluorophore	Alzheimer's disease model via prefrontal cortex injection	Anal. Chem. **2021**, 93, 11337
W1	0.077 μg/mL	Ratiometric Fluorophore (ACQ)	N/A	Dyes Pigm. **2022**, 197, 109874.
TB-BChE	39.24 ng/mL	Ratiometric Fluorophore (AIE)	Nonalcoholic Fatty Liver Model Healthy Mouse Model	J. Mater. Chem. B, **2022**, 10, 4254

DX-2	0.08 U/mL	Fluorophore	Tumor Model	Anal. Chim. Acta, **2022**, 1235, 340540
Chy-1	0.12 ng/mL	Fluorophore	Alzheimer's disease model via prefrontal cortex injection Healthy Mouse Model Tumor Model	Anal. Chem. **2022**, 94, 39, 13498–13506
HBT-BChE	7.54×10^{-4} U/mL	Fluorophore (ESIPT-AIEE)	Zebra Fish Model	Spectrochim. Acta - A: Mol. Biomol. Spectrosc **2023**, 287 122044
BCC	**0.015 U/mL**	**Chemi-Luminophoe**	**Blood Brain Barrier Passage Capacity** **Health Mouse Model** **Tumor Model**	**This Work**

Appendix B: NMR and HR-MS Results

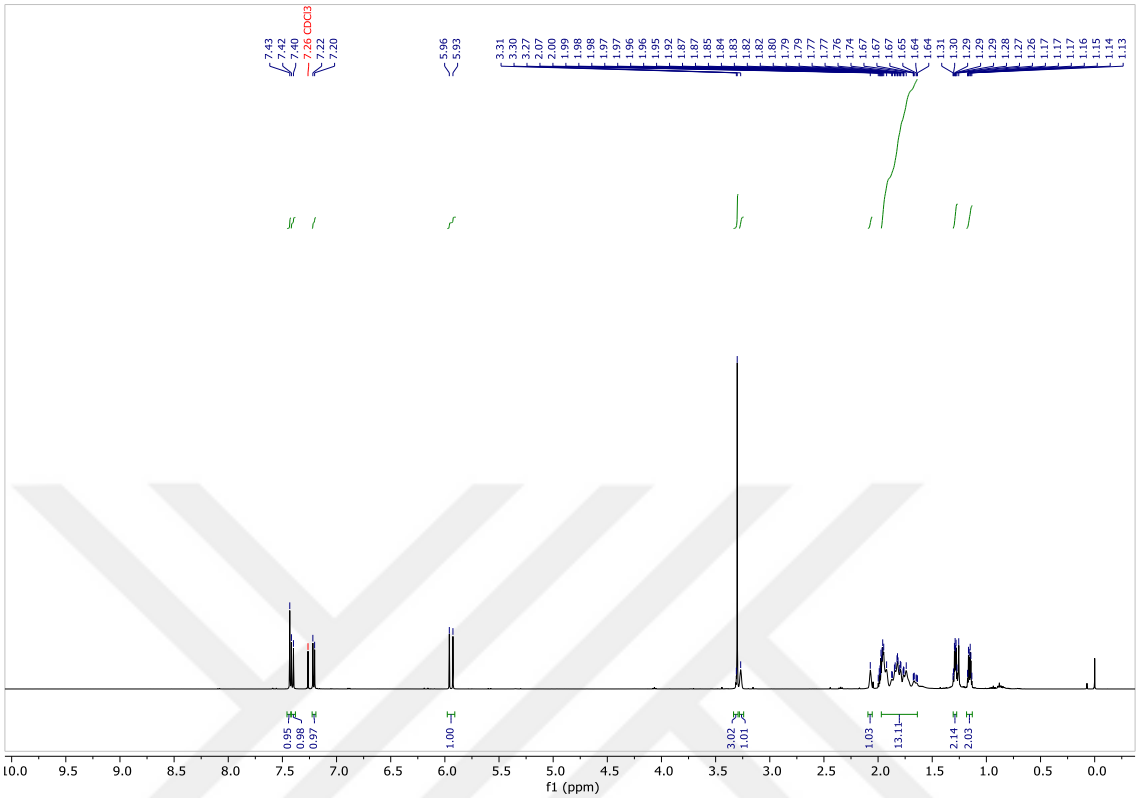

^{1}H NMR spectrum of Compound **2**.

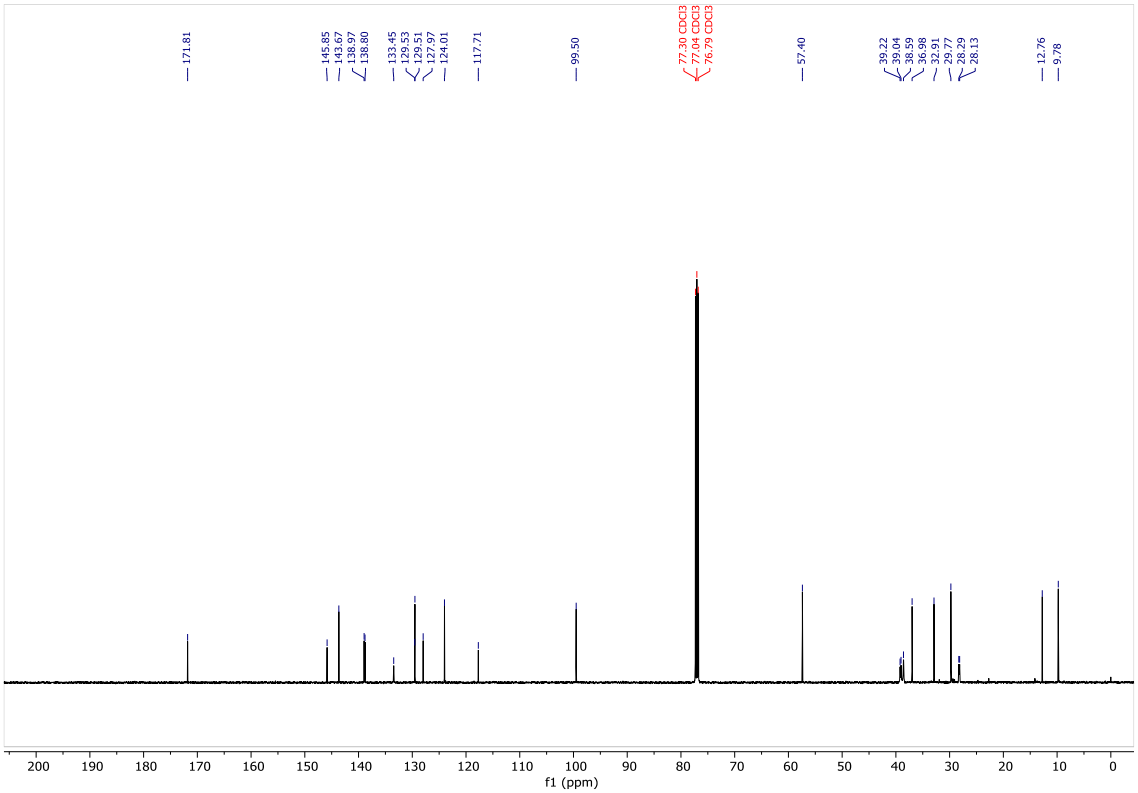

^{13}C NMR spectrum of Compound **2**.

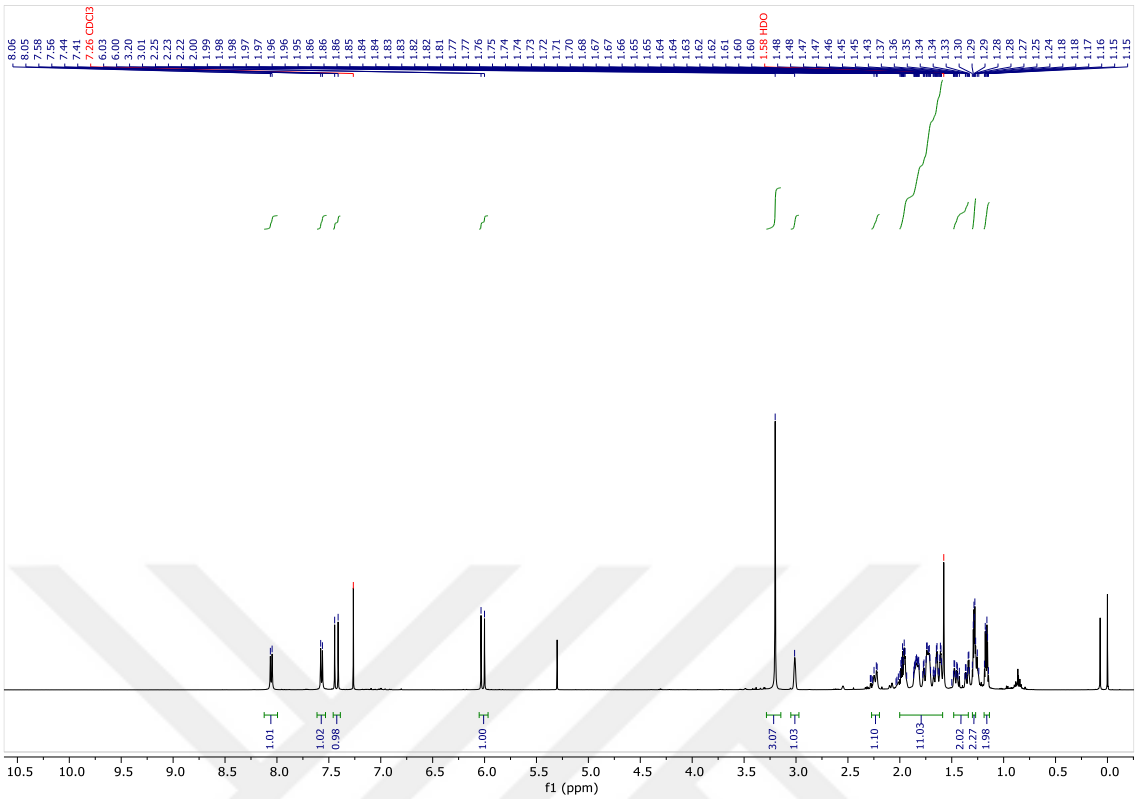

^{1}H NMR spectrum of BCC.

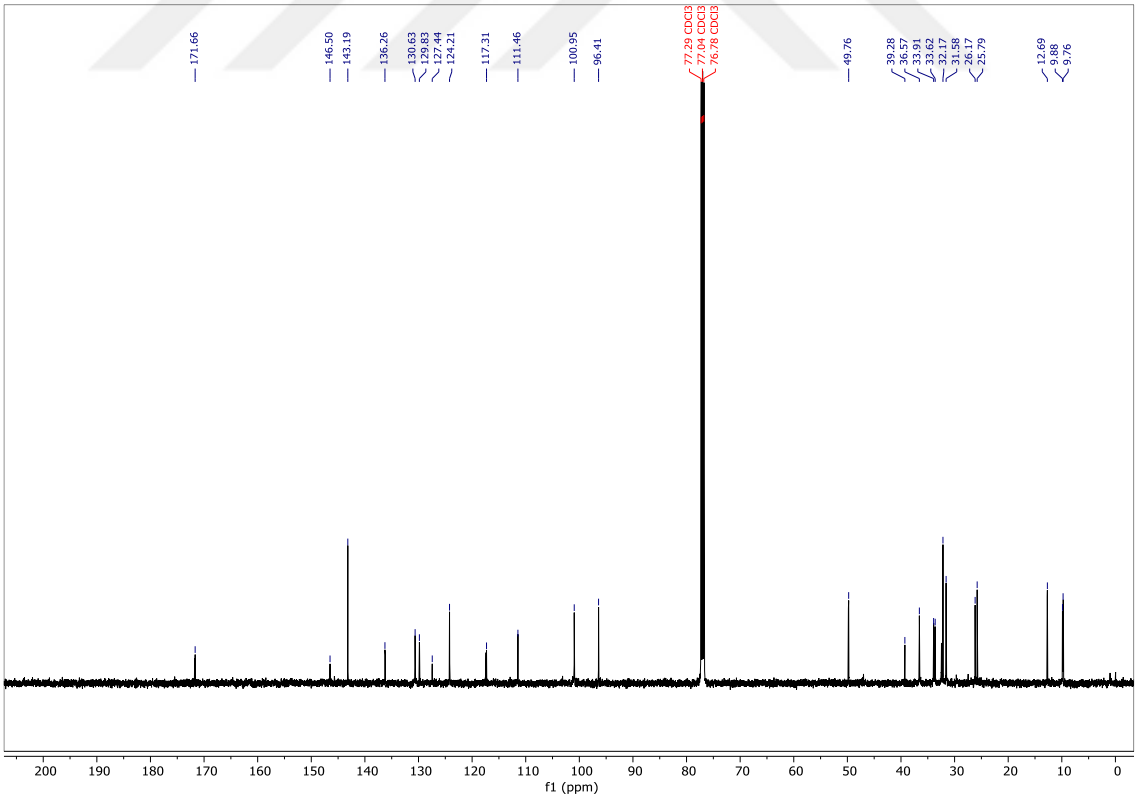

^{13}C NMR spectrum of BCC.

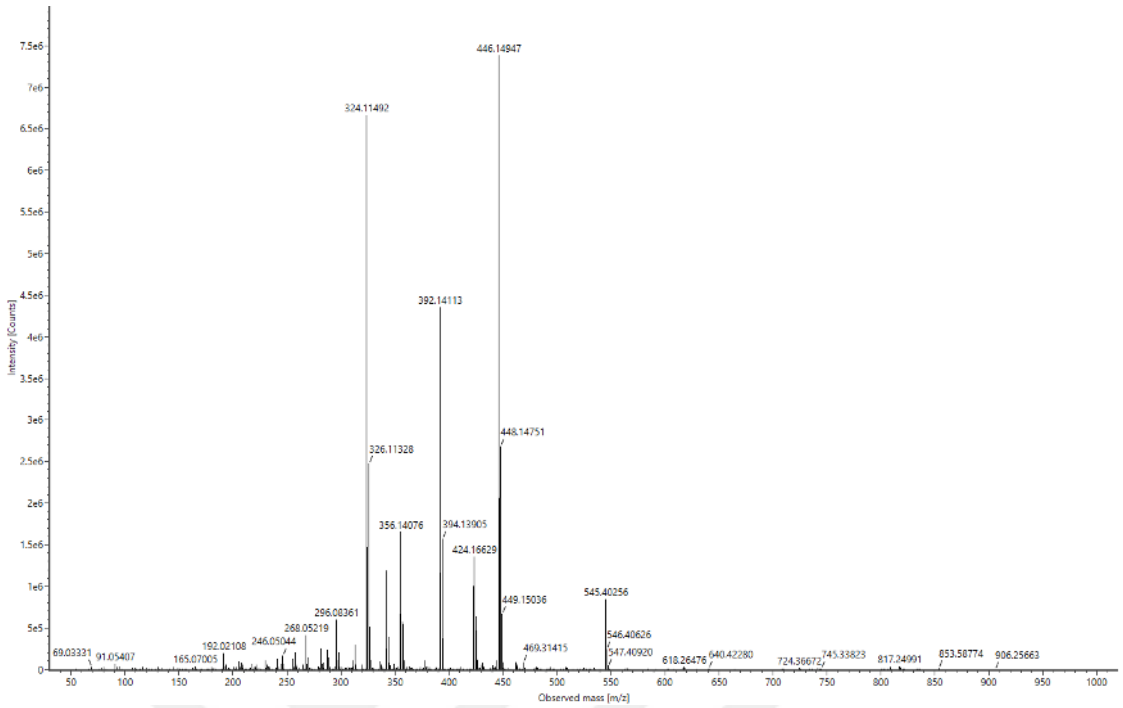

HR-MS spectrum of compound 2.